



Sea breeze interaction with urban- and mountain-induced circulations in Jakarta, Indonesia

MSc Thesis

Ashriah Andani

Supervisor: dr.ir. GJ (Gert-Jan) Steeneveld

Meteorology and Air Quality Section

Wageningen University and Research

The Netherlands

April 2022

Table of contents

Table of contents	i
Table of figures	ii
Abstract.....	1
1. Introduction	1
2. Theoretical background	3
2.1 Sea Breeze.....	3
2.2 Urban Heat Island (UHI)	4
2.3 Mountain wind.....	4
2.4 WRF-UCM.....	4
3. Methodology.....	5
3.1 Observational data.....	5
3.2 Sea breeze day selection.....	6
3.3 Model domains and grid resolution.....	7
3.4 Sensitivity analysis of WRF parameterization schemes	8
3.4.1 Parameterization schemes.....	8
3.4.2 Model evaluation	9
3.5 Isolating the influence of urban factors and mountain flow on the sea breeze	9
3.5.1 Sea breeze scaling	9
3.5.2 Factor separation approach.....	10
3.6 Influence of scale interactions	11
3.6.1 Influence on the boundary-layer dynamics	11
3.6.2 Influence on cloud formation	12
4. Results and Discussions.....	12
4.1 Sensitivity analysis of PBL and land surface parameterization schemes	12
4.2 Individual effects of mountain flow, urban factors, and the increase of SST on the sea breeze	14
4.2.1 Mountain flow influence.....	18
4.2.2 Urban factors influence	19
4.2.3 Increase of SST influence	21
4.3 Most influential factor combinations interacting with SB	21
4.4 Influence on boundary-layer dynamics	23
4.5 Influence on cloud formation	28
5. Conclusion.....	32
Acknowledgments.....	33
References	34
Appendix	38

Table of figures

Figure 1 Vertical cross-section of Jakarta city and its surrounding area in meridional (North-South) orientation.....	2
Figure 2. 1 A schematic diagram of sea breeze circulation	3
Figure 2. 2 A schematic diagram of the single-layer urban canopy model.....	5
Figure 3. 1 The surface wind analysis chart at 12:00 UTC 8th August 2018 (a), Madden–Julian oscillation (MJO) tracer map (b), and satellite image of 12:00 LT 9th August 2018 over the Jakarta coastal-urban plain (c)	7
Figure 3. 2 Three WRF domains used in this study and land use category map of the inner domain ..	8
Figure 4. 1 Time evolution of temperature differences and wind vectors during sea breeze day on 9 August 2018.....	14
Figure 4. 2 Scatter plots of SB speed characteristics within its vertical depth (y-axis) and the parameters (x-axis) according to individual factor simulations (a); and the α values of factor combinations (b).....	16
Figure 4. 3 The difference of meridional wind speed (at 10 m) at 13:00 LT between the individual effects and the flat terrain simulation.....	17
Figure 4. 4 The maximum vertical velocity of SB simulations taken at 15:00 LT with factor combinations	18
Figure 4. 5 The difference of net radiation, heat fluxes, surface air temperature, and wind speed over the urban area according to simulation with individual increase of urban factors	20
Figure 4. 6 Vertical cross-section of vertical velocity and vertical winds of the model simulations taken at 14:00 LT	23
Figure 4. 7 Vertical cross-section water vapor mixing ratio and potential temperature for the realistic case.....	24
Figure 4. 8 The horizontally averaged profile of the specific humidity	25
Figure 4. 9 The difference of boundary layer height and surface sensible heat flux between factor combination simulations and flat terrain simulation.....	27
Figure 4. 10 Vertical cross-section of cloud water mixing ratio + rainwater mixing ratio and horizontal plot of cloud liquid water path for the simulations of flat terrain, presence of topography, and increased SST.....	29
Figure 4. 11 Vertical cross-section of cloud water mixing ratio + rainwater mixing ratio and horizontal plot of cloud liquid water path for the simulations of factor combinations involving urban factors.....	31
Figure A. 1 Overview of urban characteristics in one model grid cell	39
Figure B. 1 Vertical cross-section of vertical velocity and vertical winds of the model simulations with the flat terrain and with mountains.....	40
Figure B. 2 The change of temperature (at 2 m) caused by individual factors.....	41
Figure B. 3 Vertical cross-section water vapor mixing ratio and potential temperature for the model simulations with factor combinations	42
Figure B. 4 Vertical cross-section of water vapor mixing ratio and vertical winds for a longer transect of Jakarta	43

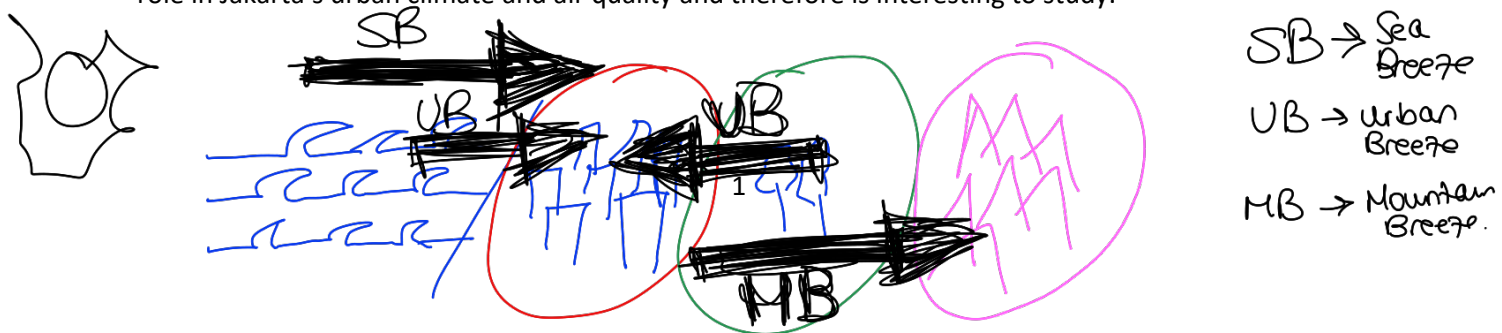
Abstract

Due to Jakarta's topographical location, different atmospheric circulations can form and interact with each other, i.e., sea-, urban-, and mountain breezes. The urbanization and sea surface temperature (SST) are projected to increase, affecting those circulations. A sea breeze (SB) case of 9th August 2018 is simulated using the Weather Research and Forecasting (WRF) model, coupled with the urban canopy model (UCM). Based on the parameterization scheme sensitivity analysis, the Yonsei University (YSU) PBL scheme and the Noah-MP land-surface can best reproduce the SB parameters. This study focuses on the influence of mountain flow, urban form (increase of building height, urban built-up fraction, and anthropogenic heat emission), and the SST increase on the SB. Thirty-two sensitivity simulations were run, consisting of five selected factors and their combinations. A sea-breeze scaling method is used to compare the impact of different factor combinations on the SB strength. Results show that the mountain flow accelerates the SB inland movement by nearly twice, while the increase of building height slightly delays the SB propagation. Combining mountain flow, the increase of urban built-up fraction, and anthropogenic heat emission results in the fastest SB propagation speed and enhanced cloud formation in the non-urban area laying over the downslope of the mountain. Meanwhile, by combining those factors with the increase of building height, the cloud lines are located closer to the city boundaries in the south. The increase of SST hinders the SB inland movement, resulting in higher boundary-layer stability and, therefore, cloudless conditions in Jakarta during a SB event.

1. Introduction

Jakarta, the capital city of Indonesia, is a densely populated coastal-urban area. It is bounded by a coastal plain in the north and a mountainous area in the south. The mountains are located about 60 km from the coastline. The city is surrounded by non-forested vegetation areas such as agricultural lands, pasture grasslands, and recreational grasses. Adjacent to the city, bare soils are found in the east and west, while forest vegetation lies in the south, close to the mountains (Robbany et al., 2019). The map of land use types in Jakarta is provided in figure 3.1.b. Given its topographical location, different forms of circulation, such as sea breeze, urban breeze, and mountain breeze potentially influence wind patterns in the boundary layer and therefore the weather system of Jakarta (Darmanto et al., 2019).

During the daytime, the sea breeze can occur due to the thermal contrast between land and sea (Miller et al., 2003), creating an onshore flow from the north sea of Jakarta. A second circulation may form as a result of the Urban Heat Island (UHI), i.e., when the air temperature in the city is warmer than its surrounding, especially starting in the late afternoon (Oke, 1995). This induces an urban breeze directed from the countryside to the city near the surface, which may hinder the sea breeze landward propagation as it moves in the opposite direction to the sea breeze. Besides, the presence of a mountainous area may induce a third daytime circulation, called a mountain breeze. When the sea-facing side of the mountain is heated, an anabatic wind current may form and potentially assist the sea breeze inland movement (Miller et al., 2003). A schematic overview of the sea-, urban-, and mountain breeze over the Jakarta area is provided in figure 1. Depending on their directions, those three circulations may strengthen or counteract each other. Their interactions can play an important role in Jakarta's urban climate and air quality and therefore is interesting to study.



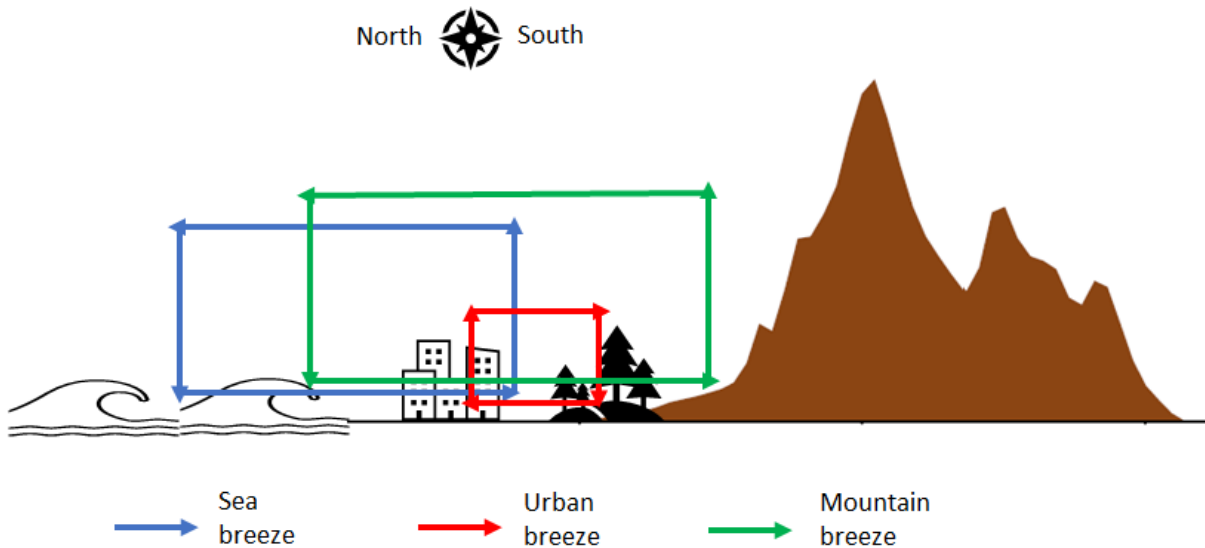


Figure 1 Vertical cross-section of Jakarta city and its surrounding area in meridional (North-South) orientation. The circulations of sea breeze, urban breeze, and mountain breeze are sketched.

Jakarta's population has annually increased by 1% during 1990-2014, and its annual growth rate is expected to become 2% in the period of 2014-2030 (United Nations, 2019). Together with large-scale housing, infrastructure, and industrial development, this has contributed to the increased urbanization over Jakarta area (Firman, 2002). Urbanization can notably impact weather patterns (Liu & Niyogi, 2019) and therefore the change of urban form can play a role in the weather system. In addition, the Ministry for National Development Planning of Indonesia (2010) projected the increase of sea surface temperature (SST) by 0.01°C to 0.02°C per year, starting in 2000. The SST increase may reduce the sea breeze inland movement due to a smaller land-sea thermal contrast. It may also impact the change of sea breeze strength. Hence, this study investigates the influence of mountain-induced flow, the urban factors, and the SST increase on the sea breeze properties.

Jakarta's rainfall variability is dominated by the diurnal cycle induced by sea breeze (mesoscale) and urban-related circulation (micro-scale) (Yamanaka, 2016). However, there is a gap of knowledge regarding the interaction between these processes. Despite many previous sea breeze studies in Indonesia, the influence of sea breeze on cloud formation and the boundary-layer dynamics has not received much attention. In a broader context of the study area, previous studies have not widely been focused on the sea breeze structures (Stephan et al., 1999). To the author's knowledge, for the Jakarta area, the interaction between sea breeze and urban circulation has only been studied by Ferdiansyah et al. (2020) based on geostationary satellite observations. The satellite-based technique has a limitation that it is only applicable when those circulations are associated with the cumulus cloud-lines presence. Besides, the orographic effects from the mountains in the south of Jakarta have not been studied yet. To circumvent the constraints related to the remote-sensing data limitation, we propose a numerical weather prediction study. The Weather Research and Forecasting (WRF, Powers et al., 2017) model coupled with an Urban Canopy Model (WRF-UCM) is a mesoscale model that can accurately represent the physical processes in urban environments located in the lower boundary layer (Bhati & Mohan, 2016; Rafael et al., 2019). It has been widely used as a compact numerical model to study the urban climate (Powers et al., 2017; Chen et al., 2011). Given its capabilities, this model is utilized in this thesis research by taking into account the boundary -layer properties, land-surface processes, urban-related factors, and mountain flow that could significantly impact the sea breeze circulation.

The main purpose of this study is to quantify and identify the influence of the interactions between sea breeze, urban-induced circulation, and the mountain flow to the boundary-layer dynamics and cloud formation over Jakarta. To arrive at the main purpose, three stages of analysis that are linked to

the different scales of circulations over Jakarta is conducted, which consist of: (1) evaluation of WRF boundary-layer and land surface parameterization schemes that can best reproduce the sea breeze; (2) analyzing the effects of increasing urban-related variables on the sea breeze; and (3) analyzing the influence of mountain flow and SST increase in sea breeze propagation.

This thesis structure is organized as follows: Chapter 2 provides background information and theoretical framework of the different circulations, which include sea-, urban-, mountain breeze, and an overview of the WRF-UCM model. Chapter 3 describes the methodology, comprising data and methods used for each working stage in this thesis. These include the sea breeze case selection, experimental setup, and model configuration. Chapter 4 presents the results and discussions which is organized per each working stage. Chapter 5 highlights important findings and further formulates them as conclusions. Limitations and recommendations resulted from this study pose as the last part of this thesis report. Supplementary information to the main content of the thesis is attached in the Appendix.

2. Theoretical background

2.1 Sea Breeze

The sea breeze (SB) is a mesoscale atmospheric circulation that occurs in coastal regions during the daytime because the air over the land heats up more rapidly than the air over the sea. Near the surface, this thermal difference creates a pressure gradient force (PGF) directed from the sea to the land carrying moist and colder air towards the land (Fig 2.1). The air mass converges with the warmer land air, and consequently, an upward vertical air current is created. This is usually called the SB front and is often marked by fair-weather cumulus clouds. The SB can be considered a closed system due to the conservation of mass. As the air over the land heats up near the surface, the vertical pressure gradient becomes less, then the high pressure at the top of the boundary layer is triggered. This creates a seaward return current that usually develops in the upper level above the boundary layer near 900 hPa (Miller et al., 2003).

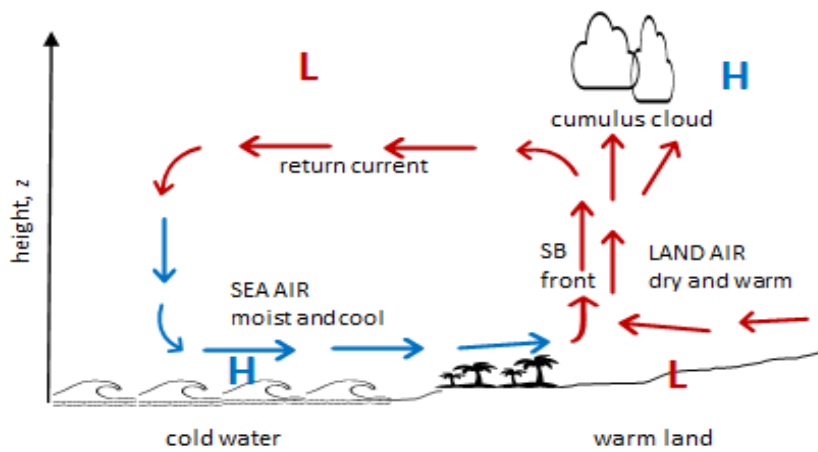


Figure 2. 1 A schematic diagram of sea breeze circulation (adapted from: Wallace and Hobbs, 2006)

In the Jakarta area, the SB can start emerging at 10:00 LT to 14:00 LT, indicated by the formation of cloud lines near the coastline. During the dry season months like August, SB may intensify in the late afternoon between 17:00 LT and 18:00 LT, with the return flow reaching 500 m to 800 m high from the surface (Hadi et al., 2002). Regarding the SB occurrence during the dry season, Miller et al. (2003) found that the calm ambient wind, including light seaward wind, is the most favourable condition for the SB inland movement in a further distance.

2.2 Urban Heat Island (UHI)

Urban heat island (UHI) is a phenomenon when the 2-m air temperature over the urban area becomes warmer than its surroundings, initiated by solar heating (Oke, 1995). This horizontal difference in surface temperature, and therefore surface air pressure, creates a circulation in which the wind flows from the non-city area towards the city, called an urban breeze, which usually starts developing in the late afternoon. For dry conditions, this horizontal thermal difference is also driven by the sensible heat flux gradients (Hidalgo et al., 2010), which is also one of the driving factors of the sea breeze. The UHI intensity depends on the ability of an urban surface to absorb and store the heat, which is influenced by the surface roughness, building and street characteristics, built-up fraction, and anthropogenic heat production.

When a SB moves inland around over the urban surface, UHI can increase or reduce the SB. Freitas et al. (2007) found that UHI can accelerate the SB landward movement due to the enhanced convection in the urban area and make the SB persist longer over the city. On the contrary, Ferdiansyah et al. (2020) and Varquez et al. (2015) found that the enhanced updraft due to urban heat circulation could potentially cause the delay of cloud propagation in a SB system due to the substantial surface drag. The surface roughness and an increase in heat released can result in a deeper boundary layer and a stronger mixing turbulent, leading to enhanced cloud formation and growth.

2.3 Mountain wind

In the daytime, the mountain slope and the air over it get heated faster than the adjacent plain, causing the overlying air to become less dense and rise upslope. This is called anabatic flow (Wallace and Hobbs, 2006). Several studies found that mountain-induced winds can influence the sea breeze. According to Ookouchi et al. (1978), mountain flow can assist the sea breeze. On the other hand, mountain-induced circulation can also act as a barrier that delays the sea breeze inland movement. An uphill wind current, resulted from the thermal contrast between the mountain slope and the adjacent land, can assist the sea breeze inland propagation if the sea-facing hillside of the mountain is relatively close to the coast (Miller et al., 2003). This terrain feature resembles our study area, as the mountains are located around 60 km from the Jakarta coastline.

Hadi et al. (2002) studied the sea breeze in Jakarta and found that, in the late afternoon, the sea breeze intensifies when reaching the area of the mountain slope. The influence of the mountain waves could induce this late afternoon intensification. Furthermore, as the sea breeze front reached the steep slope of the mountain, the radar detected postfrontal cloud cells lying over the south of Jakarta.

2.4 WRF-UCM

The Weather Research and Forecasting model (WRF) is coupled to Urban Canopy Models (UCMs) to better represent the exchange of heat, momentum, and moisture from the urban canopy to the atmosphere. This coupling aims to improve the representation of boundary conditions in the lower levels and more accurately predict the weather in the urban environment (Kusaka & Kimura, 2004). There are three parameterization schemes in the UCM: Single layer UCM (SLUCM), multi-layer Building Environment Parameterization (BEP), and multi-layer Building Environment Model (BEM). In this thesis, we select the scheme of SLUCM (Kusaka et al., 2001), which takes into account the urban morphological parameters from separated urban facets, i.e. from the roof, wall, and road. Besides, the use of SLUCM is considered sufficient and efficient to compare the effects of the selected urban surface parameters used in this thesis, as this model costs less computation time compared to the other models.

NO BEP-BEM?

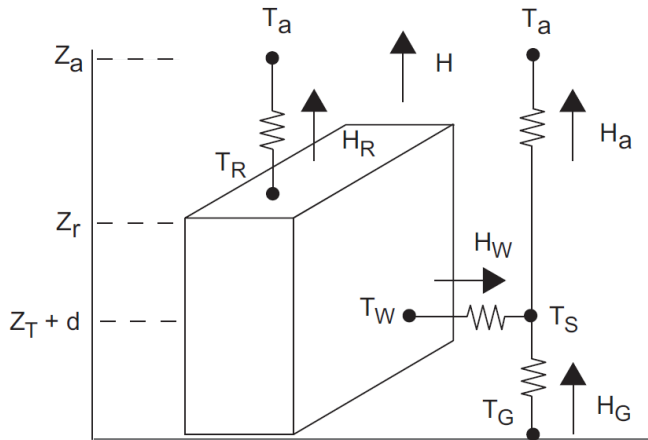


Figure 2. 2 A schematic diagram of the single-layer urban canopy model (Kusaka and Kimura, 2004)

In SLUCM, urban geometry is simplified. This model consists of features such as wind profile in the canopy, heat transfer for building parts, absorption and reflection of radiation components, and shadowing from the building. A schematic diagram of SLUCM is given in figure 2.2. T_a represents the air temperature at reference height (z_a). T_R and T_w represent the roof and the wall temperature of the building. T_g represents the road temperature. T_s is the temperature in the canyon space, defined at a certain height ($z_T + d$). H is the sensible heat flux exchange at the reference height. H_a is sensible heat flux transferred from the canyon to the atmosphere, H_w is from wall to canyon, H_G is from the road to canyon, and H_R is from roof to the atmosphere (Kusaka & Kimura, 2004). As can be seen in the schematic diagram, the SLUCM solves heat fluxes exchange and the surface temperatures of the different urban facets, i.e., roof, wall, and road.

3. Methodology

This chapter starts with a brief description of surface observational data used. Subsequently, the selection of sea breeze day (SB day) is presented in the second section of this chapter. The third section describes model configuration including the domain selection as well as grid and time resolution setting. In the following sections, this chapter describes the data and methods used in the three working stages of this study which consist of: sensitivity analysis of WRF parameterization schemes; identification the influence of selected factors to the sea breeze; and analysis on the interactions between those factors to boundary layer dynamics and cloud formation.

3.1 Observational data

Surface observation data are used for the SB day selection and model verification, including surface air temperature and wind. The temperature is measured at around 2 meters above the surface, and the wind sensors are located at 10 meters. These data were obtained from meteorological stations located at three different locations (see fig 3.2.b), which consist of 1) Tanjung Priok meteorological station (WMO code 96741) which is located in the main port of Jakarta and is only 1 – 2 km away from the coast; 2) Soekarno-Hatta (WMO code 96749), located in the main airport of Jakarta around 20 km away from the coastline; and 3) Kemayoran (WMO code 96743), located in the central Jakarta, around 6 km away from the coastline. For simplicity, Soekarno-Hatta meteorological station is referred to as ‘airport station’, Tanjung Priok meteorological station as ‘port station’, and Kemayoran meteorological station as the ‘city station’.

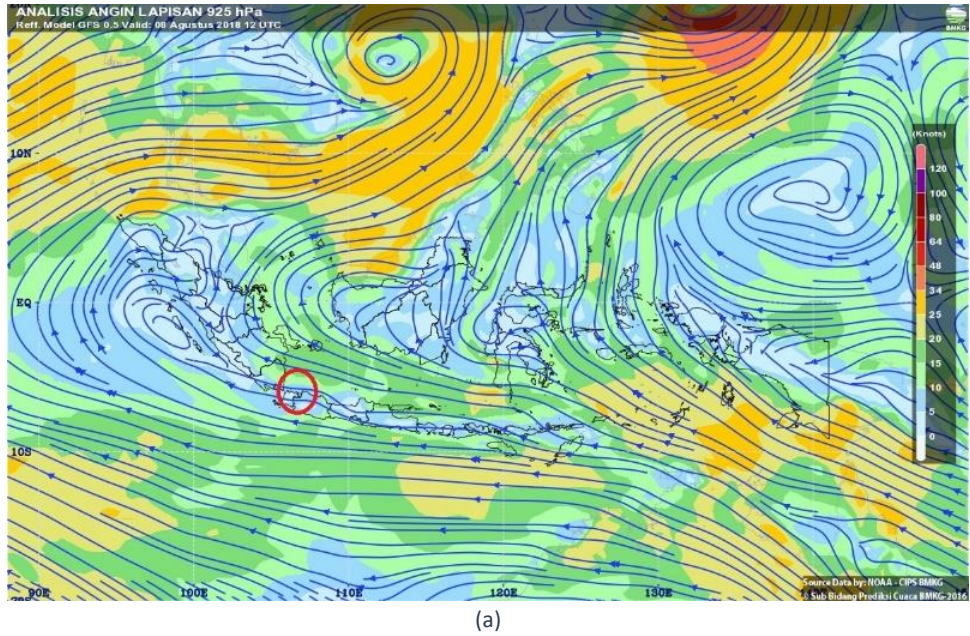


3.2 Sea breeze day selection

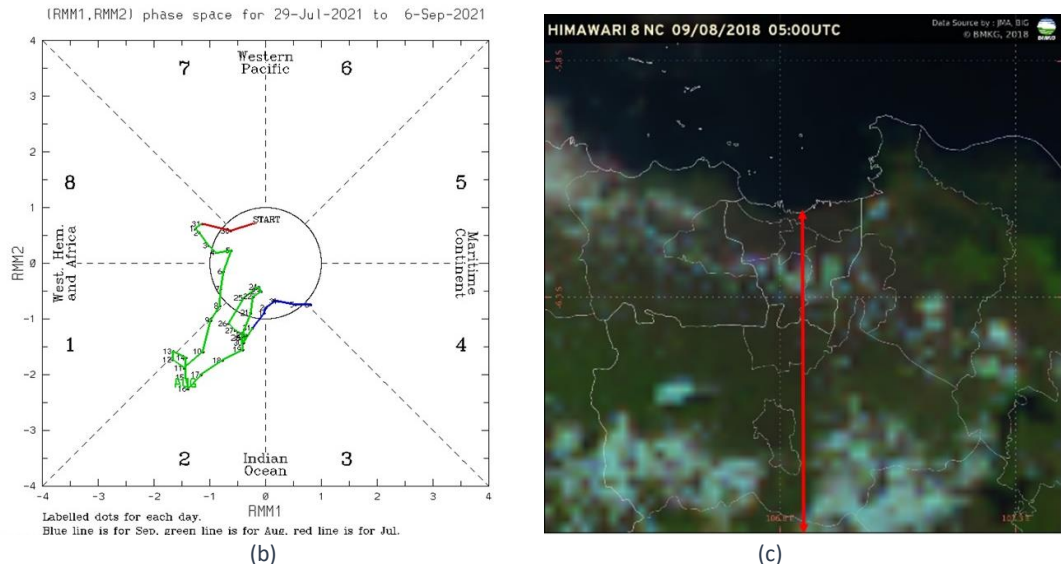
Borne et al. (1998) developed a SB day selection method that consists of six criteria as follows: (1) the change in geostrophic wind direction at the surface is less than 90° at 13:00 Local Time (LT) and 24 hours before; (2) the change of geostrophic wind speed at the surface at 13:00 LT and 12 hours before is less than 6 ms^{-1} ; (3) there is no occurrence of strong winds at 10-m level with the speed greater than 11 ms^{-1} in the daytime; (4) the daily maximum temperature difference at an inland station and a coastal station is greater than 3°C ; (5) wind direction changes at the surface exceeds 30° between the period of one hour after the sunrise and 5 hours before the sunset, and; (6) the ratio of the sharp change of wind direction (P_{peak}) and the mean change of hourly wind direction in the following 5 hours (P_{5mean}) is greater than 6. This method is based on the physical processes favourable for an ideal sea breeze formation, consisting of stable synoptic conditions, depicted by filters 1, 2, and 3, and the driving surface forces, depicted by filters 4, 5, and 6.

In this study, a SB day is adopted from previous sea breeze events in Jakarta during the dry months studied by Ferdiansyah et al. (2020). We applied all six filters in Borne's method as additional selection steps to those sea breeze events, which were originally only filtered based on two criteria: (a) the existence of wind direction changes from seaward to landward; and (b) landward wind propagation lasts for at least two consecutive hours. The data used for filtering the sea breeze day consist of surface observation data at the airport station and port station. For the upper-air meteorological variables, radiosonde data at the airport station is used. To cover the unavailability of upper-air data at the port station, we use data from the ECMWF operational analysis. This selection results in some SBDs. However, in this study, we particularly study one specific SB day of the 9th August 2018.

This SB case was chosen an example of typical SB developed along the Jakarta coast under the least effect of synoptic conditions. The surface wind analysis chart for 12:00 UTC in the day before (figure 3.1.a) shows that the synoptic wind was light easterly without convergence and shear patterns. There was no low-pressure area nor eddies observed over Jakarta and its surrounding area. The Madden–Julian oscillation (MJO), an atmospheric oscillation dominant in causing disturbances in Indonesian region was not present. Figure 4.1.b indicates that the MJO propagated in quadrant 2 which means that it prevailed over West Indian Ocean. The satellite image in the visible channel at 05:00 UTC or 12:00 LT indicates a SB on the Jakarta coastal plain (figure 4.1.c). This figure shows cumulus cloud-lines over the coast which developed after the sunrise. Over the sea, the seaward return current that usually develops in the upper level above the boundary-layer carrying the dry air mass from the land. This causes the clear skies over the sea as can be seen in the satellite image. These cloud conditions are indicative for an ideal SB occurrence.



(a)



(b)



(c)

Figure 3. 1 The surface wind analysis chart at 12:00 UTC 8th August 2018 (a), Madden-Julian oscillation (MJO) tracer map, green line is the position of MJO for August 2018 (b), and satellite image of 12:00 LT 9th August 2018 over the Jakarta coastal-urban plain, red arrow indicates distance of 60 km (c). The red circle indicates the Jakarta city and its surrounding. Source for a and c: Indonesian Agency for Meteorology, Climatology, and Geophysics (BMKG). Source for b: Bureau of Meteorology Australia (BoM).

3.3 Model domains and grid resolution

In this study the WRF mesoscale model is used to understand the boundary-layer dynamics during the sea breeze event. This study used three nested domains (figure 3.2). The reference point used for the model domain is the coordinate point of the Jakarta port station (6.132 N, 106.872 E). Our WRF model simulations use land use data from the MODIS-IGBP dataset (REF), which reads most of the Jakarta area as an urban area. Cropland and broadleaf area are present in the adjacent countryside area, and evergreen broadleaf area in the south.

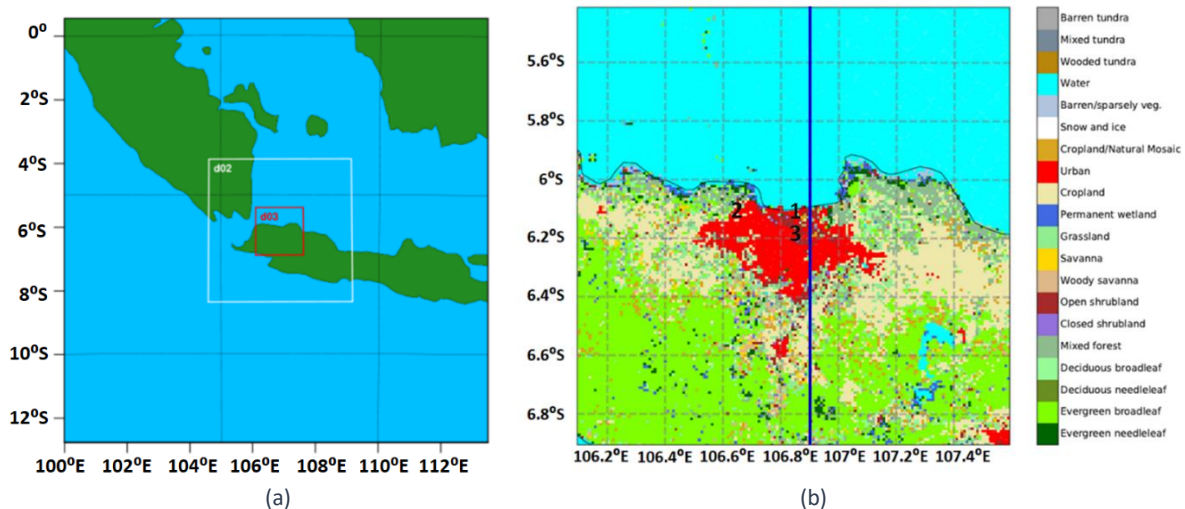


Figure 3.2 Three WRF domains used in this study (a) and land use category map of the inner domain (b). The meteorological stations marked in numbers: (1) Tanjung Priok meteorological station, referred to as 'port station'; (2) Soekarno-Hatta meteorological station, referred to as 'airport station'; and (3) Kemayoran meteorological station, referred to as 'city station'. The blue vertical line indicates the transect selected for cross-section analysis.

Given that a sea breeze is a meso- β scale (20–200 km) phenomenon (Miller et al., 2003), the domain sizes were selected based on the typical scale of sea breeze. The grid sizes of the nested domains are 9 km, 3 km, and 1 km respectively. The number of horizontal grid cells is 167x167 for all the domains, so the size of the outer domain is approximately 1500 x 1500 km². The two inner domains cover the entire Jakarta coastal area. These grid settings are adapted from the previous sea breeze studies in Antarctic Peninsula conducted by Comin & Acevedo (2017) and in China by Shen et al. (2019), for which the WRF model accurately simulated the sea breeze events. For the vertical structure, 46 eta levels are set, with the first 23 eta levels located 1.5 km to the surface, as the SB is a boundary-layer phenomenon. The lowest eta level is set at 21 m from the surface to be able to capture urban- and sea breeze and to keep the model stable when simulating the different magnitudes of urban-related factors.

The ECMWF operational analysis data were used as the input and boundary conditions, every six hours. The model was run for 36 hours for each simulation, so the ECMWF data files used were from 12:00 UTC on 8th August 2018 to 00:00 UTC on 10th August 2018. The first 12 hours are considered as the spin-up time to prevent instability of the model. The analysed part of the simulation was taken for 24 hours representing a single full day for a sea breeze event on 9th August 2018. The time step for the simulation is 72 seconds with an output frequency of 60 minutes intervals.

3.4 Sensitivity analysis of WRF parameterization schemes

3.4.1 Parameterization schemes

Since the SB is a boundary-layer phenomenon, the SB simulation might be sensitive to the selected planetary boundary-layer (PBL) parameterization within the WRF mesoscale model. Model outputs from two PBL schemes, Yonsei State University (YSU) and Mellor-Yamada-Janjic (MYJ), were compared. YSU is a first-order non-local closure scheme (Hong et al., 2006) that accounts for the exchange of turbulence properties in the atmospheric flow between the adjacent points and within points over the greater distances. MYJ, a local closure scheme (Janjic, 1994), is a 1.5-order closure with the Turbulent Kinetic Energy (TKE) prognostic equation. Arrillaga et al. (2016) compared the performance of these two schemes for sea breeze case in Northern Spain and found that both schemes tend to overestimate the wind speed during the onset of sea breeze and underestimate the

daytime temperature. In their case, YSU could simulate the wind direction change pattern in closer agreement with the observed winds. Meanwhile, MYJ produces lower temperature compared to YSU, but the temperature representation is closer to observations during the early onset of sea breeze. Both schemes, furthermore, produced rather similar pattern and magnitudes for heat fluxes. We explored the different effects of those PBL schemes produced in simulating a sea breeze circulation, especially in the tropics like Jakarta, where more heat is available.

The land-surface processes such as soil heat, soil moisture, and the canopy effects could significantly impact a SB simulation (Satyanarayana et al., 2003). The model results from the land-surface schemes of Noah (Ek et al., 2003) and Noah MP (Niu et al., 2011; Yang et al., 2011) were compared in this study. Noah covers only a single vegetation layer without an explicit canopy layer, while in Noah MP, multiple physical processes such as dynamic vegetation and canopy stomatal resistance are incorporated (Rajeswari et al., 2020). According to a comparative study on different land-surface schemes conducted by Zhang et al. (2020), Noah-MP could in their case better simulate the latent heat flux transfer compared to the other land-surface schemes, while Noah can best reproduce the sensible heat and ground heat fluxes. Therefore, it is interesting to examine whether the different performance of heat flux transfer reproduced by both schemes carries out significant work for the diurnal evolution of meteorological elements during sea breeze event in Jakarta. Four simulations with different combinations of the PBL and land-surface physics schemes were run as listed in table 3.1.

Table 3.1. Simulation runs with different parameterization set up

Simulation	PBL scheme	Surface physics scheme
1	YSU (non-local)	Noah
2	YSU (non-local)	Noah-MP
3	MYJ (local)	Noah
4	MYJ (local)	Noah-MP

Furthermore, in all model simulations, the UCM mode is activated with the single-layer urban canopy model (SLUCM) scheme (Kusaka & Kimura, 2004). The SLUCM is a two-dimensional model that includes a simplified building geometry. The overview of this urban parameterization scheme is provided in section 2.4.

3.4.2 Model evaluation

To provide a robust model evaluation, the modelled values are averaged over nine neighboring grid cells. In order to evaluate the model performance, we use various statistical metrics, which include the coefficient of determination (r^2), mean absolute error (MAE), and root mean square error (RMSE). Temperature and wind are the critical factors of the sea breeze (Ogawa et al., 2003), so these two variables were statistically evaluated with the hourly surface observation data from the airport, port, and city station as reference. The best simulation out of four, which gives the highest evaluation scores, is used as the control run for the following stages of the experiment.

3.5 Isolating the influence of urban factors and mountain flow on the sea breeze

3.5.1 Sea breeze scaling

In order to study the impact of urban factors and orography on the SB evolution, we use a sea breeze scaling method. Wichink Kruit et al. (2004) refined an empirical equation of the sea breeze strength defined by sea breeze parameters which had been previously developed by (Steyn, 1998). This equation depicts the empirical relations that are based on dimensionless variables. There are three

dimensionless parameters in this equation which consist of one parameter for the sea breeze depth and two parameters for the sea breeze strength. The relation of these dimensionless parameters is given in equation 3.1 below.

$$\text{~intensity of the SB} \quad \text{avg. WS in the SB layer}$$

$$\frac{u_{sb}}{u_s} = \alpha \pi_1^{-1/2} \pi_2^{1/2} = \alpha \left(\frac{g}{T_0 N} \frac{(\Delta T)^2}{\left(\frac{1}{t_p - t_s} \right) \int_{t_s}^{t_p} \overline{w' T'} dt} \right)^{-1/2} \left(\frac{N}{\omega} \right)^{1/4} \quad (3.1)$$

rate of work done by buoyancy during the SB

medidas

On the left-hand side, $\frac{u_{sb}}{u_s}$ is a dimensionless parameter for the sea breeze characteristics within its vertical depth. u_{sb} is the average wind speed in the sea breeze layer. In this study, u_{sb} is calculated by averaging the shoreward wind speeds within the surface to the height of 3 km. u_s is the horizontal velocity scale representing the rate of work done by buoyancy in driving the sea breeze flow defined as $g\Delta T/T_0 N$ (Steyn, 1998), where g is the gravitational constant, ΔT is the difference between land and sea surface temperature, T_0 is the temperature at sea level, and N is the Brunt–Väisälä frequency, which is taken constant as also used by Wichink Kruit et al. (2004) with the typical value of 0.016 s^{-1} .

The right-hand side terms consist of one coefficient and two dimensionless parameters. α is a coefficient representing the relation between parameters in the left- and hand-side. t_p is the present time at which sea breeze analysis is taken, t_s is the start time at which the sensible heat flux becomes positive, $\overline{w' T'}$ is the sensible heat flux, dt is the time interval, and ω is the frequency of diurnal heating. Assuming the diurnal heating takes place for 12 hours per day, the frequency of diurnal heating is calculated with the unit of s^{-1} . Implying from equation 3.1, at a fixed latitude, the sea breeze strength is a function of time-integrated sensible heat flux (Wichink Kruit et al., 2004). The influence of urban factors, mountain flow, and SST is explored by using this equation. This scaling formula was applied to several grid cells over the urban area. The alpha (α) of each factor simulations was compared to isolate the effects of individual factors and their combinations.

This sea-breeze scaling formula was validated against the observations in relatively non-complex orography, like in Vancouver, Canada by Steyn (1998) and in The Netherlands by Wichink Kruit et al. (2004). We extend the application of this scaling formula to Jakarta city, located in the tropics, using the WRF model outputs. Furthermore, we also aim to include the effect of mountain flow and urban factors on the SB more explicitly.

3.5.2 Factor separation approach → experimentos para "aclarar" los efectos de montaña, urbe y SST.

In this part of the experiment, the best parameterization schemes setup based on the sensitivity test is used as the default model setup. There are five variables tested in this factor separation analysis which consist of the presence of the mountain, three urban-related factors, and the increase of sea surface temperature (SST). The selected urban factors are part of the urban canopy model (UCM) variables, consisting of the increase of building height (ZR), urban fraction (FRC.URB), and anthropogenic heat (AH).

In order to isolate the influence of the mountains, in the baseline run (named as f_0), mountain and topography are 'flattened out'. For the urban factors, the default building height or the roof level (ZR) for the high-densely built area in WRF is 7.5 m. According to the Governor of Special Capital Region of Jakarta (2014), the maximum building height allowed for residential, office, and trade areas is 20 m, assuming an average of 5 m per story. Therefore, the value for ZR is changed to 20 m in this study. The default urban-fraction used in this study is 0.51, meaning that in a grid cell categorized as urban land use, 51% of the area in that grid is the impervious component, and the other 49% is vegetated. There is no previous research and data found about urban fraction for the Jakarta area. Therefore, in this simulation, the urban fraction is increased to 0.9 in the sensitivity study, which indicates that the

model grids that read as urban land use consist of 90% urban area, assuming the increase of urbanization. AH emissions over Jakarta area are projected to increase in 2050 with the annual average of emission ranging from 20 Wm^{-2} to 70 Wm^{-2} (Varquez et al., 2021). The default AH value for a high-densely built area in WRF-UCM is 50 Wm^{-2} . The changed value used is therefore taken from maximum AH emission, which is 70 Wm^{-2} . These values of UCM variables are spatially constant over the grids that are categorized as ‘urban’ land use based on MODIS-IGPB map. The overview of urban characteristics in one model grid cell for urban area is given in figure A.1 in the Appendix. As projected by the Ministry for National Development Planning of Indonesia (2010), the SST increase may reach 3 K in the year 2050. The factors tested, their default and modified values or conditions, are summarized in table 3.2.

Table 3.2. Default and modified values or condition of tested factors

Factor	‘Default’ value or condition	Modified value
Mountain	‘flat’ terrain	Mountains present
Building height (ZR)	7.5 m	20 m
Urban fraction or Built-up fraction (FRC_URB)	51%	90%
Anthropogenic heat (AH)	50 Wm^{-2}	70 Wm^{-2}
Sea surface temperature (SST)	Default, read from the initial atmospheric conditions	Increased by 3 K, for the model grids read as ‘water’

A factor separation approach (Stein & Alpert, 1993) is applied to distinguish the influence of those factors and their possible combinations. Since we have five variables, there are 32 model runs required to separate and rank the influence of each factor and their combinations. Output variables from these model simulations are calculated using the sea breeze scaling formula (equation 3.1). We compare the alpha (α) values of all simulations to investigate the influence of each factor combinations on enhancing or hindering the sea breeze. The scenario names, configurations, and mechanisms are given in table A.1.

3.6 Influence of scale interactions

Apart from using the factor separation approach (section 3.5.2) to analyse the factors’ influence to the sea breeze strength, we also used the same approach to explore their influence on cloud formation and boundary-layer dynamics. We isolated the influence of interactions between sea breeze and urban-induced circulation, mountain flow, and the SST increase, to the variables involved in the processes related to the clouds and boundary-layer properties.

3.6.1 Influence on the boundary-layer dynamics

Without disturbances, convection can actively occur due to solar heating. The passage of sea breeze can induce more convection as the colder air from the sea flows over a warm land surface, causing a more well-mixed boundary layer. However, the cold air reduces the boundary-layer height (Ribeiro et al., 2018; Ferdiansyah et al., 2020). Besides, urban surface affects the sensible heat, latent heat, and other boundary-layer features. The interaction between sea breeze and urban effects might influence the activity of the sea-surface sensible heat flux, which is one of the important driving forces of boundary-layer evolution (Arellano et al., 2015). We compare the model output variables comprising the surface heat fluxes as the driving force of boundary-layer evolution, boundary-layer height, vertical profiles of temperature and moisture.

3.6.2 Influence on cloud formation

An upward air motion, generated by the convergence of the relatively cold and humid air mass from the sea breeze, and warmer and dryer air from the land, may lead to low-level cumulus cloud formation under a sufficiently humid environment (Stull, 2012). Ferdiansyah et al. (2020) found that the cloud-lines passage formed parallel to the coastal area could be associated with the sea breeze inland penetration. Variables related to the properties of clouds obtained from the model outputs, including cloud water mixing ratio, rainwater mixing ratio (QRAIN), and liquid water path (LWP) integrated from vertical levels of model output. These variables are analyzed for different factor combination simulations and thus the effects of factor combinations on cloud formation are isolated.

4. Results and Discussions

In this thesis, we simulate the essential influence of factors upon which the SB depends. This chapter is started by the results and discussions of the sensitivity analysis of WRF PBL and land-surface schemes. The best combination of PBL and land-surface schemes is used as the model parameterization scheme setup in the factor separation analysis which consists of 32 simulations. Secondly, the results of factors' influence according to the scaling and vertical velocity analysis are presented. This is followed by further analysis of individual factors' influence of mountain flow, the increase of building height, urban fraction, anthropogenic heat, and SST. Moreover, the most influential factor combinations in strengthening and obstructing the SB, isolated from factor separation, are discussed. In the next section, the influence of most influential factor combinations on the boundary-layer dynamics is analysed. This demonstrates the influence of interactions between SB, mountain flow, urban factors, and the increase of SST. At last, the analysis of most influential factor combinations to the cloud formation is explored.

4.1 Sensitivity analysis of PBL and land surface parameterization schemes

Four simulations with different combinations of PBL and land-surface parameterization schemes, as listed in table 3.1, were run for our SB case. Table 4.1 shows the statistical evaluation metrics of simulated surface air temperature and wind speed compared to the observation. In general, correlation shows that models can reproduce the temperature and wind in a good agreement with the observations, with the correlation scores above 0.8 for the temperature in all simulations and above 0.5 for the wind speed. The changes of wind direction to be more landward, indicating the onset of the SB, from all simulations also fairly correspond with the observed winds (figure 4.1.b and d).

Table 4. 1. The statistical evaluation scores of the 2-m surface air temperatures and 10-m wind speed between WRF simulations and observations for the SB case on 9th August 2018 for all the three (port, city, and airport) meteorological stations

	YSU_Noah	YSU_NoahMP	MYJ_Noah	MYJ_NoahMP
Temperature (°C)				
Correlation (r (-))	0.91	0.87	0.89	0.88
Bias	-1.41	-0.43	-1.04	-0.16
MAE	1.53	1.03	1.36	1.12
RMSE	1.73	1.25	1.63	1.35
Wind speed (ms⁻¹)				
Correlation (r (-))	0.56	0.62	0.54	0.55
Bias	0.77	0.68	0.83	0.82
MAE	1.14	1.07	1.33	1.39
RMSE	1.57	1.51	1.85	1.94

In our SB case, both PBL YSU and MYJ schemes tend to underestimate the surface temperature and overestimate the wind speed. This behaviour of these two schemes was also found in the other SB study taking place in Northern Spain by Arrillaga et al. (2016) and in Indian tropical station by Boadh et al. (2016). For the temperature, the MYJ results in a cold bias (i.e., observed-simulated < 0) compared to YSU. Similar comparison was also found in the study of Northern Spain, while in Indian tropical station both schemes did not show significantly different bias. Higher MYJ temperatures (compared to YSU) can be explained by the ability of MYJ, a local closure scheme, which can capture the local process like the thermal convection during the day better than the non-local scheme. Therefore, it produces higher temperatures compared to YSU. However, when combined with land surface Noah-MP scheme, MYJ overestimates the temperature at the SB passage (see figure 4.1.a and c).

Despite its ability to capture more local processes within the boundary layer, in our SB case, MYJ results in a higher bias in wind speed compared to YSU (see table 4.1). This is also confirmed by the validation scores in which MYJ gives slightly lower correlations and greater errors. YSU, a non-local closure scheme, accounts the exchanges of turbulence properties in the atmospheric flow, not only between the adjacent points but also the points over the greater distances. This means that by using YSU scheme, the model also considers the non-local vertical transport. Therefore, YSU can better reproduce the wind which values are closer to the observation compared to MYJ, especially in a mesoscale phenomenon like sea breeze.

In our SB case, the most notable difference resulted between land surface Noah and Noah MP is that Noah MP scheme can produce better agreement of simulated surface temperature compared to the observation. Noah MP tends to reproduce higher temperature compared to Noah. This is because Noah MP simulates higher soil moisture and latent heat flux (not shown), causing the evaporation to be higher, and therefore higher temperature (Zhang et al., 2020). It can be related to the ability of Noah MP scheme to calculate physical processes in multiple vegetation and canopy layers. Better performance of Noah MP can also be seen in the simulated wind speed, although the bias and errors are not significantly different compared to Noah.

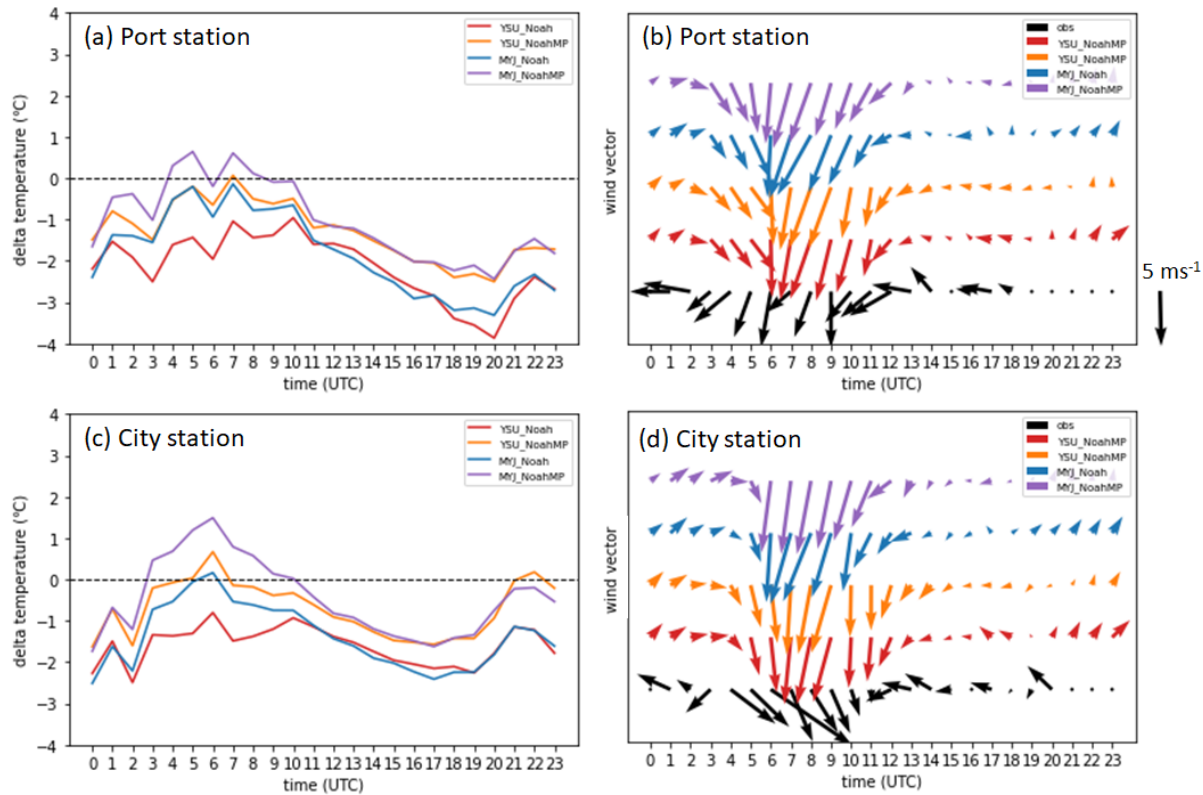


Figure 4. 1 Time evolution of temperature error and wind vectors during sea breeze day on 9 August 2018 at the port station (a and c) and at the city station (b and d) based produced by model simulations with different PBL and land surface parameterization schemes. North wind direction indicates landward wind flow.

Overall, the combination between PBL YSU and land surface Noah MP was found to best reproduce temperature and wind during our SB case, considering the statistical evaluation scores and the wind patterns at the SB passage. The RMSE for the temperature and wind are 1.25 K and 1.51 ms⁻¹ respectively. Additionally, the daytime temperature also corresponds best with the observed temperature, both in the port and city stations (see figure 4.1. a and c). This parameterization setup is used for the factor separation analysis with 32 WRF simulations. Furthermore, it is important to note that this parameterization scheme sensitivity analysis was done towards a realistic case simulation, which is with the mountains present, as well as default values for urban factors and SST. This simulation is referred to as f1 in the next sections.

4.2 Individual effects of mountain flow, urban factors, and the increase of SST on the sea breeze

In the reference model simulation (f0), the topography in the model domains including the mountains in the south of Jakarta, is flattened. This means that there are no motions induced from the mountains and is as such comparable to cases for which the SB scaling has been validated over the flat terrain in earlier studies, e.g., in the Netherlands by Wichink Kruit et al. (2004). For this 'flat terrain' simulation, the characteristics of the urban factors and the SST are set to default (see section 3.5.2). This baseline simulation infers that the wind turns from offshore to onshore at 03:00 UTC or 10:00 Local Time (LT) which denotes the onset of SB (not shown). The SB constantly intensifies in the following hours and its penetration reaches the distance of 30 km from the coastline by the end of the afternoon. The model output indicates that SB develops significantly during 13:00 LT to 15:00 LT (see figure B.1 in the Appendix). Thus, the scaling analysis using equation 3.1, was done for those time steps from the model outputs.

The coefficient α in equation 3.1, referred to as 'alpha' in this thesis, denotes the relation between SB characteristics within its vertical depth and the parameters including surface temperature and the time-integrated sensible heat flux. The values of alpha can be used to compare the SB strength in different cases or locations (Wichink Kruit et al., 2004). In this thesis, we use the values of the alpha to compare the SB strength produced by simulations with the different factors and their combinations. A higher alpha indicates a stronger SB over the coastal urban plain, since the sample points to calculate the alpha are taken mostly over the coastal urban area.

Figure 4.2.a shows the scatter plots and the alpha values of individual factors according to the sea breeze strength scaling. The alpha values from all the factor combinations are presented in figure 4.2.b. We find that, over the Jakarta coastal plain, the mountain flow (f1) appears to accelerate the SB, shown by a steeper slope and higher value of the alpha which is almost twice than the reference alpha (f0). This implies that the orography can strongly accelerate the SB propagation. Meanwhile, the resistance from the urban canopy through the increase of building height and the increase of SST can interrupt the SB. The increase of SST (f5) most significantly hinders the SB compared to the other individual factors. Among the urban factors, only the increase of building height (f2) slightly obstructs the SB inland movement. This delayed penetration can only be visible at 15:00 LT, at which SB delays the SB penetration by 2.8 km (not shown). Meanwhile, the increase of urban fraction (f3) and the increase of anthropogenic heat (4) do not result to noticeable impacts to the SB speed, based on their alpha values.

In general, factor combinations involving the increase of SST result in smaller alpha values compared to the other combinations, meaning that the increase of SST plays a substantial role in slowing down the SB inland penetration. This applies for both the simulations with and without the presence of mountains. The second factor that also contributes to the SB movement obstruction is the increase of building height, although the effect is less substantial than the SST increase. Out of all the factor combinations, the combination of mountain flow, the increase of urban fraction and the increase of anthropogenic heat (f134) results to the highest alpha value. This means that the interaction of SB and mountain flow, with the increase of built-up urban area from 51% to 90% with the building height remains default as 7.5 m, and the anthropogenic heat emission increases from 50 Wm^{-2} to 70 Wm^{-2} , most accelerates the SB inland movement.

In addition to the scaling analysis, which represents the SB strength in the vertical column (from surface to 3 km level), we further examine the surface wind patterns produced by the factor simulations. Given that the shoreline orientation of Jakarta is in the east-west direction, we use meridional wind component (v) to analyse the SB landward propagation. The negative v indicates the wind blowing to the south, which in this case, means that the wind blows from the sea to the land. Meanwhile, positive v means that the wind blows in the opposite direction. We analyse the change of meridional wind pattern as the effects prescribed by individual factors. This is performed by taking the difference between the individual factor simulations and the reference (flat terrain) simulation. The effects of individual factors on the SB inland penetration speed can be seen in figure 4.3.

INTENSIDAD DE LA BRISA DE BIDA

A LOS DIFERENTES FACTORES (MONTAÑA⁽¹⁾) CIUDAD⁽²⁻⁴⁾
Y SST(⁽⁵⁾) VIENE DADO POR α

$$\alpha_{f_0} = 0.91$$

$\alpha > \alpha_{f_0} \Rightarrow$ mayor SB max. Strength

$\alpha < \alpha_{f_0} \Rightarrow$ menor SB max. Str.

$$[\cdot]_{\text{SB max. Str.}}$$

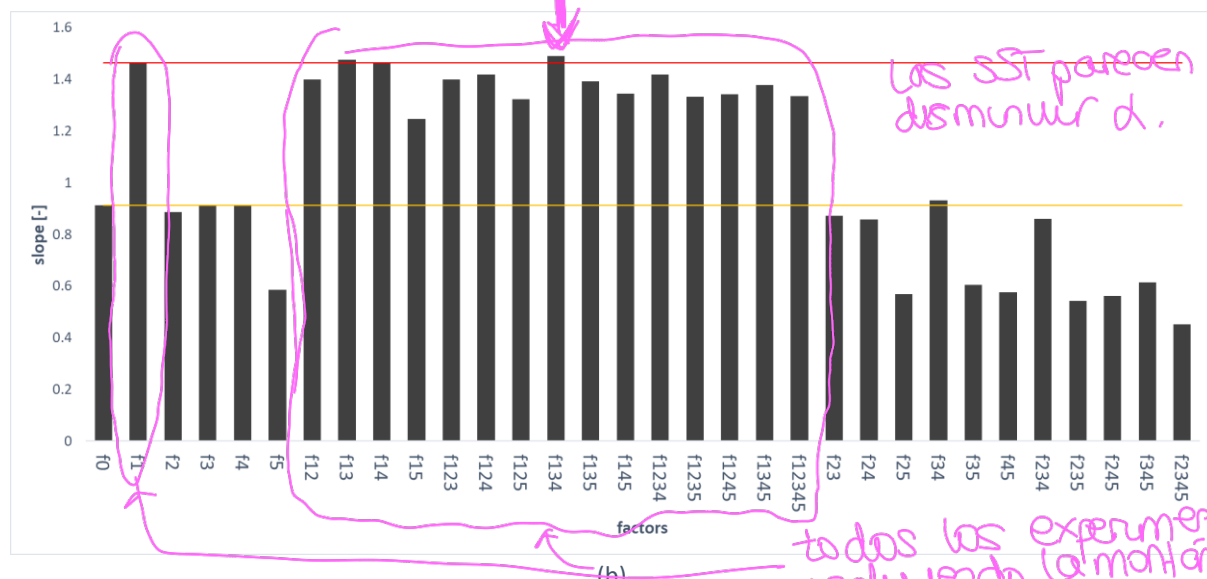
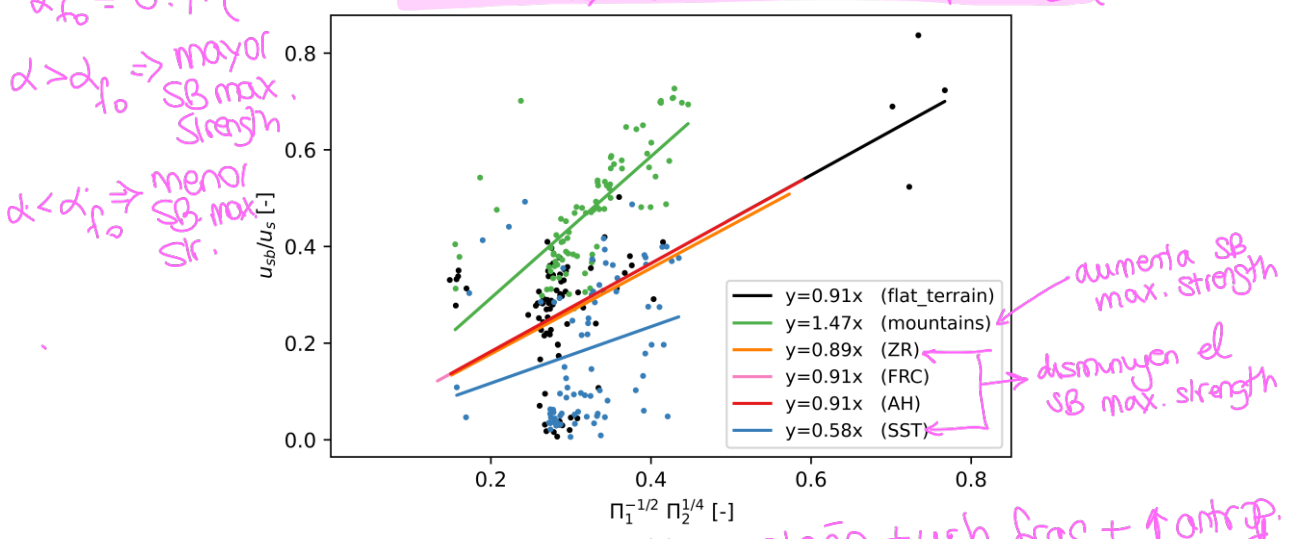


Figure 4. 2 Scatter plots of SB speed characteristics within its vertical depth (y-axis) and the parameters including surface temperature and the time-integrated sensible heat flux (x-axis) according to individual factor simulations (figure a); and the alpha (coefficient α) of SB simulations taken at 13:00 LT to 15:00 UTC (figure b). Alphas are calculated with zero intercept. Factor numbers in the horizontal axis are indicated as follows: 1. the presence of mountain; 2. the increase of building height (ZR); 3. the increase of urban fraction (FRC_URB); 4. the increase of anthropogenic heat (AH); and 5. The increase of sea surface temperature (SST). The red and yellow horizontal lines are auxiliary lines to help comparing the alpha with the reference simulations of the flat terrain and with the mountains.

The change of meridional 10-m wind generally confirms the results shown by the scaling analysis. The mountain flow accelerates the SB inland movement with the increase of speed up to 8 ms^{-1} close to the coastline. The increase of SST hinders the SB by up to 7 ms^{-1} over the coastline. By increasing the building height from 7.5 m to 20 m, landward wind over the urban area slows down by about 4 ms^{-1} . Besides, the increase of anthropogenic height speeds up the SB to a slight extent over the downtown.

Edificios más altos
reducen SB en la
zona urbana.

$$\Delta(\sqrt{v_{ref}} - \sqrt{v_{fa}}) \begin{cases} < 0 \Rightarrow (azul) \Rightarrow SB \uparrow \uparrow \\ > 0 \Rightarrow (rojo) \Rightarrow SB \downarrow \downarrow \end{cases}$$

(intensidad)

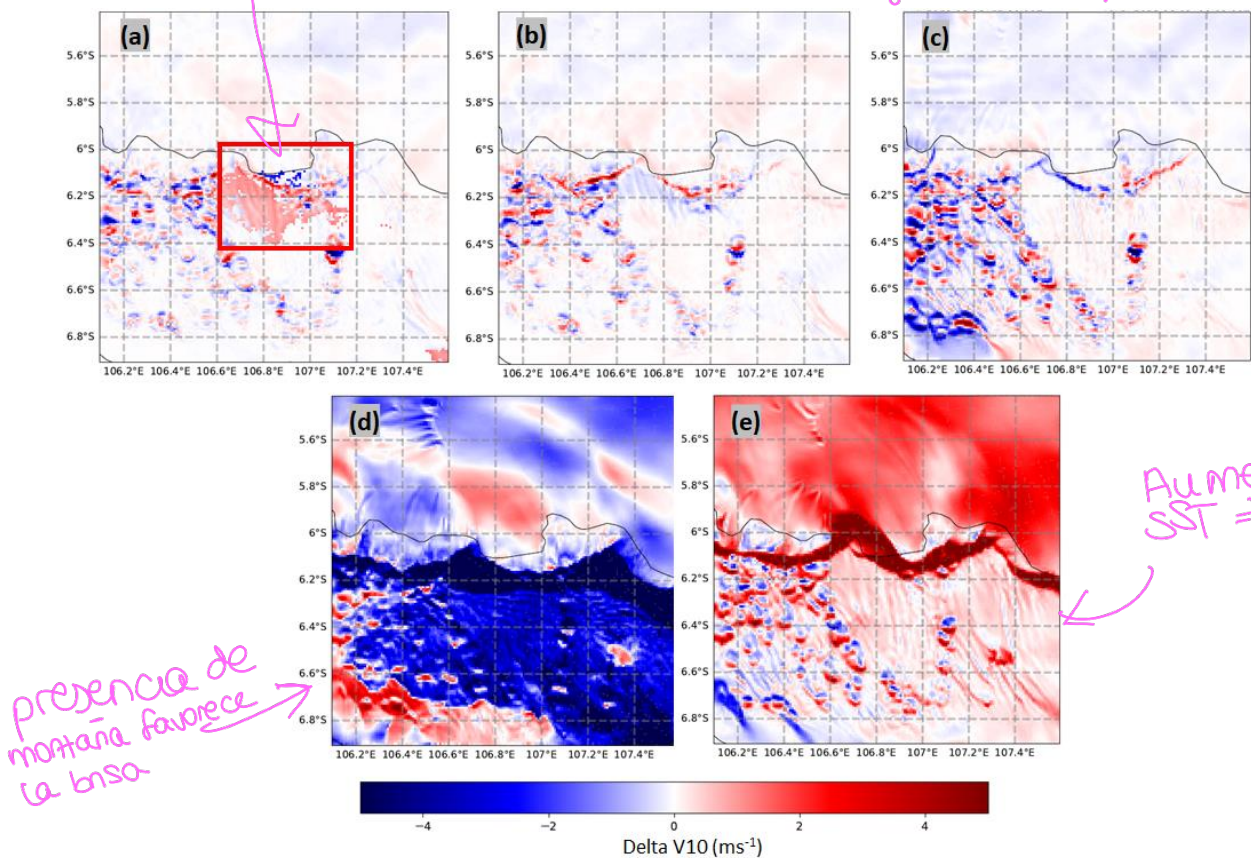


Figure 4.3 The difference of meridional wind speed (at 10 m) at 06:00 UTC (13:00 LT) between the individual effect of the increase of building height (a), the increase of urban fraction (b), the increase of anthropogenic heat (c), the presence of mountain flow (d), and the increase of sea surface temperature (e), compared to the reference simulation. Red shade (positive difference) shows the wind blowing more seaward compared to the reference. Blue shade (negative difference) shows the wind blowing more landward. The red rectangle indicates the urban area.

Aside from analysing the SB strength, we explore the SB frontal system rendered by the vertical motion of the air. We compare the maximum vertical velocity produced by factor simulations. The maximum values were taken from the vertical column of a transect in meridional orientation. The transect area is shown in figure B.1 in the Appendix. Figure 4.4 shows that the orographic effect from the mountain slows down the upward motion by $\sim 1 \text{ ms}^{-1}$, which is rather substantial in magnitude compared to the typical value of vertical velocity, which can range from 1 to 3 ms^{-1} for a condition with cumulus clouds presence (Lohmann et al., 2016). The SST increase also hinders the vertical air motion by nearly the same magnitude as caused by the mountain flow. The increase of each of the urban factors enhances the updraft by 1 to 2 ms^{-1} . Note that these values are simulated for the SB case under the least influence of synoptic conditions during the dry season, so that vertical air movement is not associated with synoptic scale convergence or substantial surface pressure systems. The magnitude of vertical velocities depends on the SB frontal zone and the rate of SB front inland development (Helmis et al., 1987). Therefore, we can conclude that higher vertical velocities were determined by the stronger SB frontal system. The individual strongest effect enhancing the upward motion is given by the increase of urban fraction, which in this case, we change the urban built-up fraction from 51% to 90%. Further discussions on the individual factor effects and most influential factor combinations are discussed in the following sections (section 4.2.1 - 4.2.3).

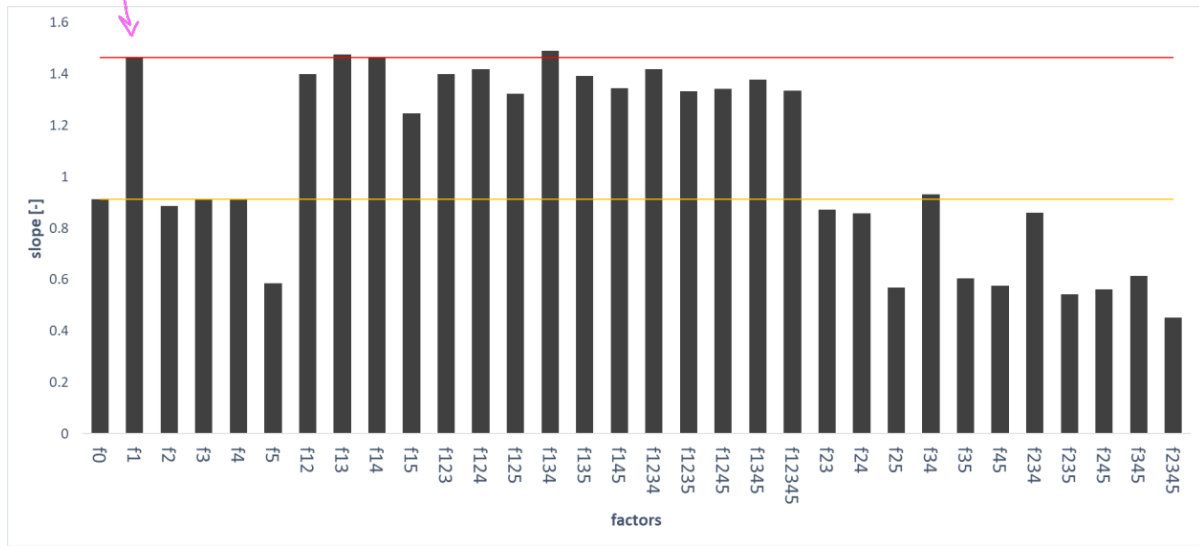


Figure 4.4 The maximum vertical velocity of SB simulations taken at 08:00 UTC (15:00 LT). Factor numbers in the horizontal axis are indicated as follows: 1. the presence of mountain; 2. the increase of building height (ZR); 3. The increase of urban fraction (FRC_URB); 4. The increase of anthropogenic heat (AH); and 5. The increase of sea surface temperature (SST). The dashed lines are auxiliary lines to help comparing the alpha values with the reference simulations with the flat terrain and with the mountains.

4.2.1 Mountain flow influence

The mountains in the south of Jakarta, located around 60 km from the coast, appears to influence the SB properties. Table 4.1 shows the inland propagation of SB according to the model simulations with the flat terrain and with the presence of mountains, indicated by the location of SB front. It can be inferred that the mountain flow enhances the SB propagation speed with a factor of about two according to the SB case simulation. On the same diurnal cycle of the coastal land-sea thermal heating, during the daytime, the sea-facing hillside of those mountains is heated and subsequently, anabatic flow is created. In our SB case, this flow assists the SB inland movement near the surface (Miller et al., 2003). The cross-sectional plot of the SB front locations is provided in figure B.1 in the Appendix. The SB front is located more to the south when SB interacts with the mountain-induced flow. At 17:00 LT the SB front already ceases to be visible as it encounters the mountain slope, even though the near-surface landward flow still exists.

Table 4.1. The comparison of SB front location between model simulations with and without the effects of mountains.

Hour (Local Time)	Distance of SB front from the coastline (km)	
	Flat terrain	With mountains
12:00	-4.0 (over the sea)	8.4
13:00	6.3	12.1
14:00	12.4	21.3
15:00	18.0	31.9
16:00	23.4	44.2
17:00	28.1	Not visible

In the simulation with mountains present, aside from the SB moving towards the mountains, anabatic winds are created in the steep slope of the mountain, leading to the acceleration of SB inland movement near the surface. The upslope winds occur earlier than the formation of SB system over the coastal plain (see figure B.1 in the Appendix). Next to that, the southern part of Jakarta urban area and the adjacent vegetated area in the south of the city lies above the edge of the mountain slope

with the elevation ranging from 50 m to 200 m. These areas and the mountains heat up faster compared to the flat terrain simulation which read the mountainous area as flat-vegetated land. The presence of mountains causes warmer temperature over the land, compared to no-mountains. Therefore, the land-sea temperature contrast is higher, leading to a stronger SB.

Aside from accelerating the near-surface SB movement, the mountain flow slows down the vertical air motion in the SB front for simulation at 15:00 LT. As the accelerated SB transports colder air mass, it reduces the city air temperature more rapidly compared to the SB in the flat terrain condition (see figure B.2 in the Appendix). Therefore, the available heat is less than the flat terrain condition. Further discussion on the boundary-layer stability condition, which is related to the strength of updraft in the SB front, is given in section 4.4. Moreover, as a higher amount of cold air advected by the accelerated SB, the thermal difference between urban area and the surrounding decreases, resulting to a weaker UHI effect (Ribeiro et al., 2018). Near the surface, the SB and the mountain-induced horizontal flow move in the opposite direction to the urban breeze (see figure 1.1). This competition between accelerated SB and the urban breeze could dilute the updraft in the SB front. Even with less effect of UHI, the SB front updraft in the mountains-condition is still weaker than the flat terrain condition. This implies that the boundary-layer profile more strongly determines the strength of SB front updraft, rather than the competition between SB and urban breeze.

4.2.2 Urban factors influence

In the flat terrain and realistic simulations (with mountains), increasing the building height in urban areas results in colder city temperature. When there is more urban fabric, more heat is stored in the concrete buildings and less heat is put in the atmosphere. This temperature change can also be related to the delayed SB penetration and a slower upward motion in the SB front caused by building height increase. With the increase of built-up fraction, the city temperature becomes colder at the SB passage but warmer in the city part where SB is inactive. An increase in anthropogenic heat emission slightly increases the city temperature. The horizontal maps of these temperature differences can be seen in figure B.2 in the Appendix.

To analyze the change of surface air temperature and heat fluxes in the city, we take the average of the change of these variables in all grid cells of the urban area. In the daytime, by increasing the building height from 7.5 m to 20 m, the urban surface air temperature and upward sensible heat flux decrease. Meanwhile, the upward ground heat flux increases, meaning more heat is transferred upwards (see figure 4.5). We also calculated the net-all wave radiation (Q^*) from the summation net shortwave radiation and net longwave radiation in WRF outputs. By the increase of building height, the daytime changes of Q^* and latent heat flux are not substantial. As the ground heat flux increases, upward sensible heat flux is decreased due to surface energy balance. The temperature decreases because it is proportionally related to sensible heat flux. This colder urban temperature explains the delayed SB penetration, indicated by a slower landward wind speed (see figure 4.3.a). The surface energy balance used to explain this model behavior is given in equation 4.1.

$$\text{Net_SW} + \text{Net_LW} + \text{AH} = \text{HFX} + \text{LH} + \text{GRDFLX} \quad (4.1)$$

The left-hand side term is the net all-wave radiation (Q^*), calculated from the summation of net shortwave radiation (Net_SW) and net longwave radiation (Net_LW), and anthropogenic heat flux (AH). The right-hand side terms are the sensible heat flux (HFX), latent heat flux (LH), and ground heat flux (GRDFLX). The unit for all terms is in Wm^{-2} .

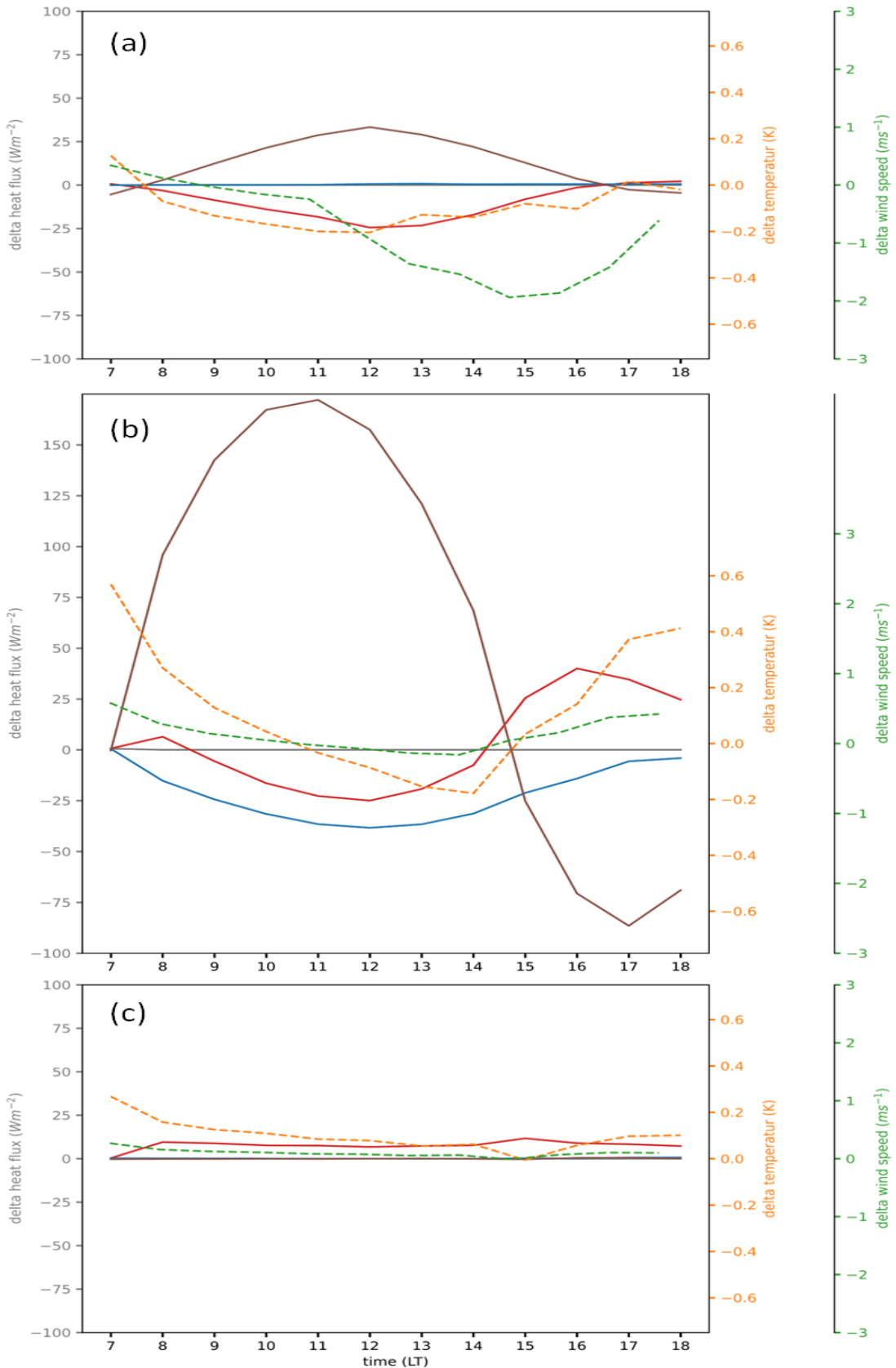


Figure 4.5 The difference of net radiation, heat fluxes, surface air temperature, and wind speed over the urban area according to simulation with: (a) building height increased; (b) built-up fraction increased, (c) anthropogenic heat emission increased. The primary vertical axis range in figure (b) is made different from the others due to a large ground heat flux difference value.

With the increase of urban built-up fraction from 51% to 90%, the daytime ground heat flux greatly increases. This increase is compensated by the decrease of sensible and latent heat fluxes. Unlike the increase of building height simulation, the temperature only decreases when the SB penetrates further inland when the SB carries colder air temperature. This indicates that a higher built-up fraction can store more cold air transported by SB compared to less built-up urban area. The simulation with the increase of anthropogenic heat emission from 50 to 70 Wm^{-2} in the city results to a slight increase of urban sensible heat flux during the daytime, ranging from 7.6 – 8.6 Wm^{-2} . This leads to a slight increase in surface air temperature. However, the increase of urban built-up fraction and anthropogenic heat in our case do not significantly influence SB propagation and upward vertical velocities.

4.2.3 Increase of SST influence

SB would not form without the land-sea temperature contrast, as this thermal contrast is one of the most critical factors influencing SB development. The increase of SST delays SB inland propagation by about 5 km (not shown). The land-sea temperature difference becomes lower and, therefore, the weaker forcing for the SB shoreward movement. Apart from slowing down the SB propagation, the increase of SST also results in a weaker vertical air motion in the SB front at 15:00 LT (see figure 4.4). At this hour, the SB front is located over the downtown due to its delayed penetration. This delayed SB propagation entrains a lower amount of colder air from the sea. Compared to the reference simulation (default SST), the surface temperature at the SB passage is even higher, as the SST is warmer. As the city is warmer than the reference, the heat contrast between city and non-city is higher. This induces the formation of UHI circulation in front of the SB front. As SB and urban breeze flow in the opposite direction, the UHI could contribute to suppressing the SB front updraft.

4.3 Most influential factor combinations interacting with SB

We focus on the realistic case, where the orographic effect occurs, given that the mountains are present in the south of Jakarta in real-life conditions. Therefore, in this section, we further analyse the factor combinations with the mountain presence that are most influential in accelerating (f134) and hindering the SB (f15). We also analyse f1234, which is the only factor combination that can increase the upward motion in the SB front. For the sake of clarity, the description of factor combinations is given as follow:

- a) **f0**: a simulation with the flat terrain (mountains are flattened out), the urban factors and SST are set to their default values (building height 7.5 m, urban built-up fraction 51%, and anthropogenic heat emission 50 Wm^{-2});
- b) **f1**: a realistic case with the presence of mountains in the south of Jakarta, the urban factors and SST are set to their default values
- c) **f134**: a simulation with mountains present, and the urban built-up fraction and anthropogenic heat are increased;
- d) **f1234**: a simulation with mountains present, the building height, urban built-up fraction, and anthropogenic heat are increased. Therefore, in the urban area we have 90% built-up area (and thus only 10% vegetated), the buildings are 20 m high, and the anthropogenic heat emission is 70 Wm^{-2} ; and
- e) **f15**: a simulation with mountains present, with urban factors set to default, and SST increased by 3 K.

In the flat terrain simulation, SB front is located over the city centre (18.4 km from the coastline, see table 4.2). Simulations with the presence of mountains result in farther distances of SB front from the coast but slower updraft in the SB front, as explained in section 4.2.1. Simultaneous increase of the

urban built-up fraction and anthropogenic heat emission results in the fastest SB propagation but slower updraft. However, increasing the building height and other urban factors enhances updraft, although the SB inland movement is slightly delayed than the unchanged building height. The combination between mountain-induced flow and the increase of SST results in a significant delay of SB penetration and lower upward vertical motion in the SB front.

Table 4. 2. The comparison of SB front locations and maximum vertical velocities between most influential factor combinations at 15:00 LT

	f0	f1	f134	f1234	f15
Location of SB front from the coastline (km?)	18.4	33.4	36.5	33.4	21.9
Maximum vertical velocity at SB front (ms^{-1})	2.9	2.1	1.9	2.4	1.3

In all selected simulations above, the cross-sectional maps (figure 4.6) show that there are two updraft systems in the SB front. Each is located adjacent to the SB front and in the cold air behind the SB front. The first is the primary updraft, induced by the convergence between denser air mass from the sea and lighter air from the land. The latter is formed due to mass conservation and can also be intensified by thermal instability. This updraft marks the size of SB circulation (Miller et al., 2003). Apart from accelerating the SB, mountain flow also increases the size of SB circulation (see figure 4.6.a and b).

By increasing the urban built-up fraction and anthropogenic heat emission (f134), another updraft forms in front of the SB front, around the border of the city and noncity area (see figure 4.6.c). This could be induced by the urban breeze circulation, as the extra heat over the city and higher city-noncity thermal contrast are favorable to form UHI. The presence of urban breeze could dilute the SB as it flows in the opposite direction to the SB near the surface, slowing down the updraft in the SB front. Nevertheless, the interaction between the SB and urban breeze also results in a slightly larger horizontal area of the updraft.

By increasing the building height, meaning that all selected urban factors are simultaneously increased (f1234), the UHI-induced updraft is not visible (see figure 4.6.d). When only primary updraft arises, without obstruction from the UHI, the upward vertical velocity in the SB front is higher by 0.5 ms^{-1} compared to unchanged building height (f134). This indicates that the UHI could interrupt the upward motion in the SB front. However, it is difficult to certainly judge the presence of UHI due to the model's ability to capture such a local phenomenon in our model resolution. Nevertheless, vertical velocity becomes even larger than the value of the reference simulation (f1). The increased building height could cause higher surface friction, adding thermal instability and strengthening the updraft. Further discussion of the boundary-layer dynamics is given in section 4.4.

The combination of mountain-induced flow and the increase of SST was found to hinder the SB inland movement and the updraft velocity. At 15:00 LT, the SB front location with the increased SST is 11.5 km behind the SB front with the unchanged SST. This is caused by a weaker sea-land thermal contrast as SST increases, resulting in a slower SB speed. An updraft in front of the SB front was found (figure 4.6.e), indicating that the city-noncity thermal contrast is sufficient to form the UHI, as the southern part of the city is still not passed by the SB. For the simulation with the increase of SST, we could also conclude that a weak updraft results from a weak SB and the obstruction from the seaward-moving urban breeze.

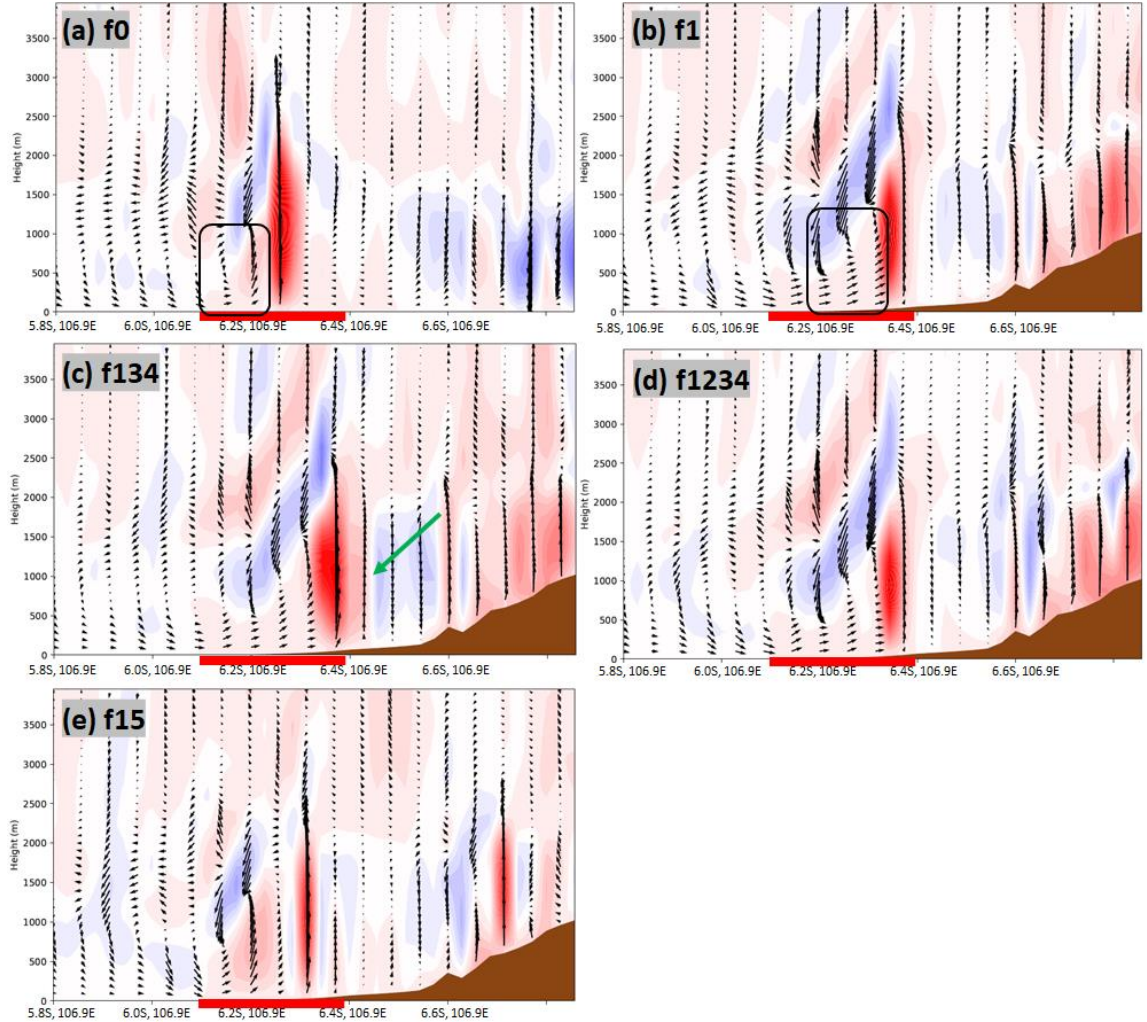


Figure 4. 6 Vertical cross-section of vertical velocity (shaded) and vertical winds (arrows) of the model simulations taken at 07:00 UTC (14:00 UTC), produced by simulations: (a) with flat terrain; (b) with the presence of mountains (realistic case); (c) realistic case with increased urban built-up fraction and anthropogenic heat emission; (d) realistic case with increased of all selected urban factors; and (e) realistic case with increased of SST. Red line indicates the urban area. Black rectangles indicate the area of SB circulation. The green arrow indicates the UHI-induced updraft.

4.4 Influence on boundary-layer dynamics

In analysing the boundary-layer dynamics, we focus on simulations with the presence of mountains (f1) and most influential factor combinations, as discussed in section 4.3. To analyse the influence of the mountain, we compared f1 with the flat-terrain simulation (f0) which has all urban factors and SST unchanged. To isolate the effect of urban factors and SST, we compare f1234, f134, and f15 to the realistic case simulation (f1). The boundary-layer properties analysed are boundary-layer height, sensible heat flux, potential temperature and specific humidity, which can be interpreted from the water vapour mixing ratio.

In the realistic case simulation, that is with the presence of mountains, and values of urban factors and SST set to default, the model shows that the potential temperature (Θ) increases with height (figure 4.7). In the early morning, the isentropes are tightly assembled in the vertical cross-section which denotes more statically stable atmosphere. This condition also applies for all selected scenarios (see figure B.3 in the Appendix). This is indicative for our SB case which occurred when the effect of large-scale disturbances was least present.

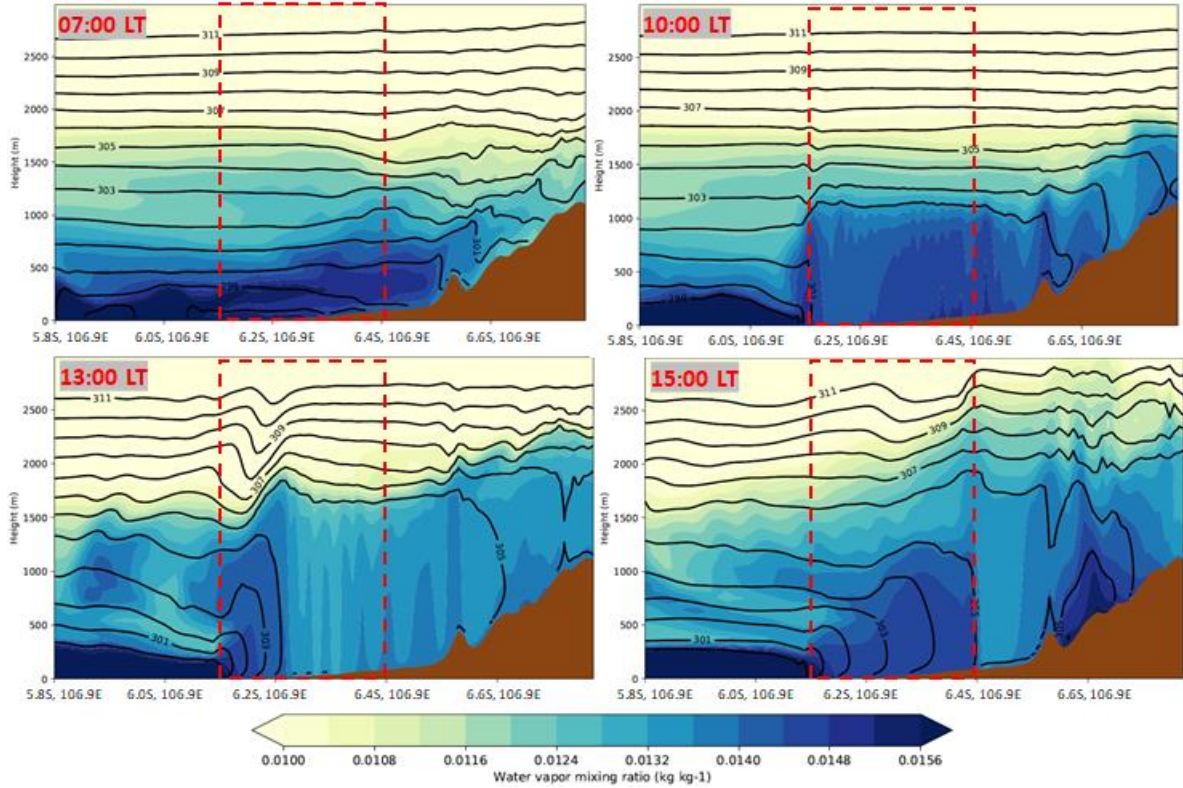


Figure 4.7 Vertical cross-section water vapor mixing ratio (shades) and potential temperature (contours) for the ideal case (f_1) at 07:00 LT (00:00 UTC), 10:00 LT, 13:00 LT, and 15:00 LT. The red dashed rectangle indicates the city cross-sectional area, over which the horizontally averaged profiles are taken.

Over the city, the boundary-layer depth increases from roughly 100 m in the early morning to about 1700 m at 13:00 LT (not shown). As the surface becomes warmer, moisture is transported by thermal convection to the boundary layer top. From the surface until around 1500 m above the city, the isentropes are spaced further apart, meaning that the potential temperature only changes very slightly with height. This well-mixed column indicates boundary layer depth over the city, with the top at about 1600 m from the surface according to our model output. The vertical cross-section (figure 4.7) shows a downward-like motion of drier air mass at 13:00 LT, particularly over the centre and southern part of the city. Even though the individual eddies, that could form as the results of downward moving air masses surrounding the thermal plumes, cannot be captured by our WRF simulation with the resolution of 1 km. These downward moving air masses contain dry air entrained from the free atmosphere (Arellano et al., 2015). The mixing of these plumes causes the column from the surface to the top of the boundary layer to become more well-mixed as heat and moisture are well-distributed, indicating a low static stability condition. At noon, in the northern part of the city over which the SB passes, the air gets colder and moister than the southern part of the city. The boundary layer thereby becomes shallower as the SB transports colder and moister air mass from the sea.

To better capture the change in mixing profile over the city influenced by the SB and its interaction with the other factors, we analyse the horizontally averaged specific humidity profiles based on the cross section. The meridional cross-sectional transect, which indicates the urban area, used to average the specific humidity is depicted in figure 4.8. In the realistic case, figure 4.8.a shows that surface layer is moister than the upper layer. As the solar radiation becomes more intense in the next hours, surface becomes drier than before. The specific humidity remains relatively constant with height until about 1500 m from the surface. After the SB already passes the whole part of the city, at 15:00 LT the air within that layer is cooled and turning back into moister air.

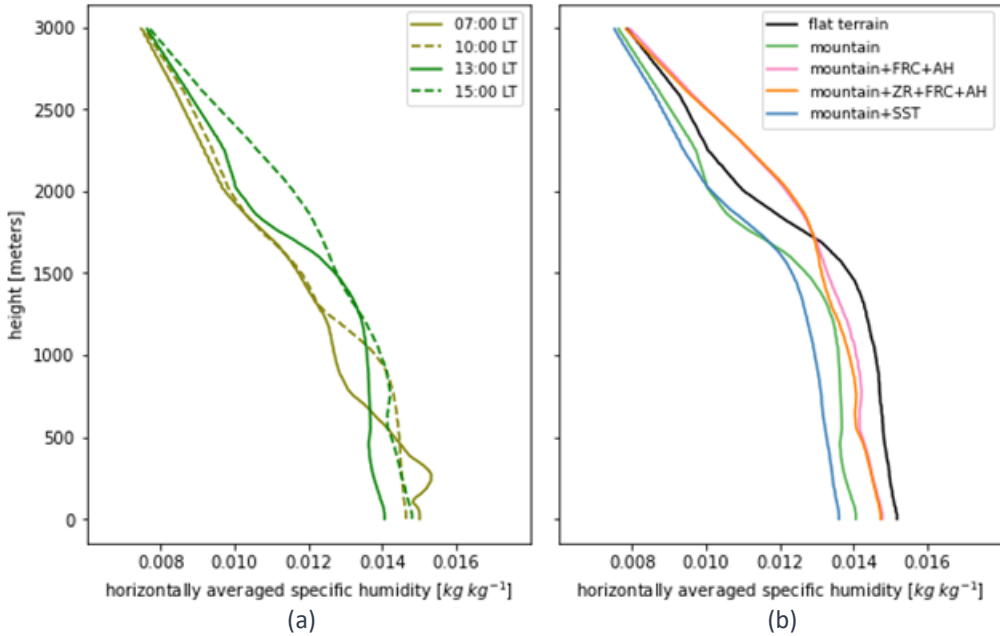


Figure 4.8 The horizontally averaged profile of the specific humidity based on the cross-section. Left panel shows the model simulations for the realistic case (with mountains) at the different time steps. Right panel shows simulations for the different scenarios at 13:00 LT.

According to figure 4.8.b, the vertical mixing of the boundary layer produced by different factors and their combinations can be inferred. The presence of mountains results in drier air within the boundary layer compared to the flat-terrain condition, although the accelerated SB should carry a higher amount of moister air. The entrainment of drier air from the free troposphere is more enhanced in the simulation with the mountains present (see figure B.3 in the Appendix), which contributes to additional drying within the boundary layer. In the mountain slope, the air mass rises and cools as the surrounding air temperature decreases with height. This return current is what we see as the downward motions over the city (see figure B.1.f in the Appendix). These mountain-related processes could be the cause of the colder and drier air mass over the city. The well-mixed layer, and therefore the boundary-layer depth, is shallower compared to the flat terrain simulation.

To explore the other processes causing a drier boundary layer with the presence of mountains compared to the flat terrain simulation, we inspect a larger meridional cross-sectional transect. This is due to the fact that the mountains lie between the Jakarta area (northern Java coast) and the West Java area (southern Java coast). Apart from the SB coming from the northern coast, there is another SB current flowing from the southern sea (in the south of West Java) moving towards the north (see figure B.4 in the Appendix). The flat terrain simulation clearly shows that this northerly SB flow transports the water vapor to the land part, reaching the ‘flattened’ mountainous area. Besides, the model reads this area as a vegetated area, which adds up the water vapour availability over the land boundary layer. Due to these reasons, the flat terrain simulation reproduces the moister boundary layer. The presence of mountains blocks this moisture transport further to the Jakarta urban area, which results in the drier boundary layer.

When increasing the built-up fraction and anthropogenic heat emission, the city is heated more quickly than before. A warmer city air advances the SB inland movement, and therefore the city air mass becomes moister as the cold air from the sea is transported earlier. Consequently, the well-mixed layer is deeper, although this layer is less well-mixed compared to less urbanized conditions, shown by a little steeper slope in figure 4.6. With the increase of building height, the boundary layer is slightly drier due to a slight delay in SB propagation, especially in the level of 500 m to 1000 m.

The effect of SST increase is rather straightforward. As discussed in section 4.2, the increase of SST delays the SB propagation. At noon, the SB has not passed the city yet, which subsequently causes the urban atmospheric boundary layer to be drier compared to the default SST simulation. This is because the SB should carry a moister air mass to the city. Increasing the SST results in a slightly deeper well-mixed layer. Furthermore, compared to the realistic case (with mountains), increasing the SST causes a slightly less well-mixed boundary layer. From this, we can conclude that the higher SST results in a higher atmospheric boundary-layer stability.

Furthermore, we analyze the spatial difference of the boundary-layer depth and surface sensible heat flux in the horizontal plane produced by different factor simulations (figure 4.9.a and b). Compared to the flat terrain simulation, mountains cause shallower boundary layer over the land area between the SB front and the coastline. Over the urban area passed by the SB, the decrease of boundary-layer depth is 400 m on average. However, the sensible heat flux is higher, which is uncommon as a higher sensible heat flux should result in boundary layer growth. Due to the advection of cold and less turbulent air from the sea over the warmer land surface carried by the SB, the surface-atmosphere temperature difference becomes larger than before. As the sensible heat flux is dependent on this difference, it becomes larger compared to flat-terrain simulation. These results show that, at the SB passage, the boundary-layer depth is decoupled from sensible heat flux. Aside from the advected cold temperature, the model also takes into account the advection of boundary-layer height from the sea. The advection here refers to the meridional gradients of horizontal advection due to the fact that the SB moves from the north to the south. The advected boundary-layer height layer is shallower. This advection suppresses the boundary layer over the area where the SB is active, although a high sensible heat flux should increase boundary-layer depth.

This decoupling was also found in the model simulation with the increased SST (see figure 4.9.g and h). As the SST is higher, SB transports warmer air mass inland and therefore surface temperature over the land increases. This leads to higher boundary-layer depth over the land. By increasing the SST by 3K, the increase of boundary-layer depth reaches 400 m at the land area where the SB is active. Due to the advection of warmer air than in the reference situation, land surface-atmosphere temperature difference is smaller and the sensible heat flux as well. This is again the fact that, at the SB passage, the sensible heat flux is decoupled from the boundary-layer height during the propagation of SB.

When the built-up fraction and the anthropogenic heat over the urban area are increased, at the SB passage, the sensible heat flux is lower by averagely 23 Wm^{-2} than the less-urbanized condition. This is because the advected cold air counteracts the heat over the city. A larger built-up fraction could limit the ability of colder air to penetrate further. Therefore, the sensible heat is lower over the area where SB is active yet larger over the area in front of the SB frontal zone (see figure 4.9.d). The increase of sensible heat flux over the urban area where the SB is inactive reaches 61 Wm^{-2} . This larger sensible heat flux might also be triggered by the surplus of anthropogenic heat flux. Besides, the artificial modification of land surface, such as the increase of built-up fraction, could contribute to the increase of sensible heat flux, which leads to the UHI occurrence (Kato & Yamaguchi, 2005). The boundary layer is shallower at the SB passage and higher in the city area, where the sensible heat flux is higher due to anthropogenic heat increase.

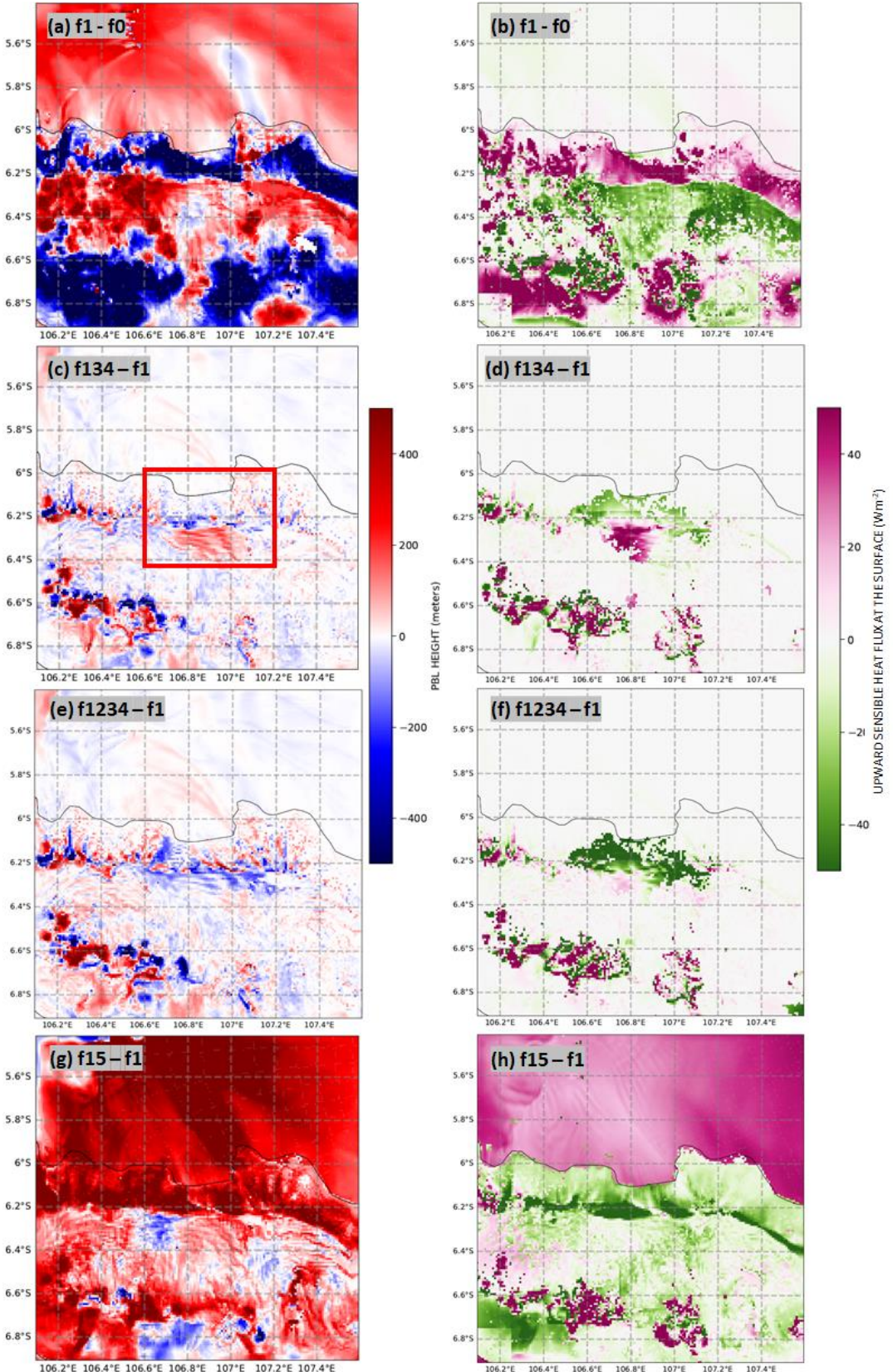


Figure 4.9 The difference of boundary-layer height (left panel) and surface sensible heat flux (right panel) between: (a and b) simulations with the presence of mountains (realistic case) and flat terrain; (c and d) realistic case with increased built-up fraction and anthropogenic heat in the urban area compared to the default urban condition; (e and f) realistic case with increased of all selected urban factors compared to default urban condition; and (g and h) realistic case with increased of SST compared to default SST condition. Differences are calculated from the model outputs at 13:00 LT. The red rectangle indicates the urban area.

Furthermore, if the building height is increased, the sensible heat flux decreases more remarkably at the land area where the SB is active (see figure 4.9.f). Meanwhile, in the city area in front of the SB front, the sensible heat flux is slightly higher. The model simulation shows the increase of all selected urban factors simultaneously results in a slightly shallower boundary-layer height in the downtown. Although a higher sensible heat flux could cause more turbulent mixing throughout this layer and therefore increase its depth, the return current of anabatic flow moving downwards suppresses the boundary layer at the same time. This downward moving flow is more intense compared to unchanged building height (see figure 4.6.c and d). These mountain-induced downward motions entrain dry air from the free troposphere to the boundary layer, which in a way can enhance the sensible heat flux (Henkes et al., 2021). Furthermore, figure 4.9.e illustrates that the boundary layer is deeper over the SB front. As the lower sensible heat behind the SB front and higher flux in front of it also converges, the boundary layer could get warmer and therefore grow deeper in the frontal zone. This can explain why the upward vertical velocity is higher when we increase all the urban factors simultaneously, compared to the other factor combinations.

4.5 Influence on cloud formation

This section contains the analysis for the same factor combinations used in the boundary-layer dynamics analysis (section 4.4). The variables analysed consist of cloud water mixing ratio (QCLOUD) representing condensed water in the clouds, rainwater mixing ratio (QRAIN), and liquid water path (LWP) which is a measure of the total mass of liquid water droplets in the atmosphere above a unit surface area. QCLOUD and QRAIN are summed up for the cross-sectional analysis. LWP is calculated for analysing the horizontal cloud distribution.

According to the model outputs in all selected simulations with an interval of one hour, clouds are present at 15:00 LT. Therefore, we perform the analysis of the clouds for that time step. At this selected time, model simulations show that the SB already moves further inland, and the vertical velocities are the highest (see section 4.2). A higher amount of moisture is available in the urban area as the SB carries moist air to the land. In our SB case, the water vapor mixing ratio within the boundary layer exceeds 15 g kg^{-1} , which indicates a sufficiently humid environment to initiate convection (Holloway & Neelin, 2009). A condition with sufficient moisture and convective air parcels is favourable for cloud formation (Lohmann et al., 2016).

According to the cross-section (figure 4.10), clouds are observable from the selected factor combinations, with the base height ranging from 1500 m to 1800 m from the surface. The vertical extent of the clouds ranges from roughly 1000 m for the realistic cases (figure 4.10.c and e, with the mountains present) to 3000 m for the flat terrain simulation (figure 4.10.a). The maximum vertical velocity in the SB front ranges from 1 to 3 ms^{-1} , which is sufficient for cumulus clouds formation (Lohmann et al., 2016). The horizontal distribution of the liquid water path (figure 4.8.b, d and f) denotes that the cloud lines follow the shape of the coastline. This gives a good indication that the clouds are associated with the SB front. This is in accordance with (Miller et al., 2003) that the SB front can provoke convective activity and is often marked by the development of fair-weather cumulus clouds.

As discussed in section 4.2, the vertical velocity over the SB front is the highest in the flat terrain simulation compared to the other factor combinations. The vertical motions associated with clouds predominantly govern the vertical redistribution of moisture (Lohmann et al., 2016). Concerning the boundary-layer conditions, the flat terrain simulation produces a moister and deeper boundary layer, suggesting a higher potential for cloud formation. These conditions lead to thicker clouds in the flat terrain simulation, with the cloud extending from an altitude of 1500 m to 4000 m. With the flat

terrain, at 15:00 LT, the SB front is located 18 km from the coastline, which is over the centre of the city.

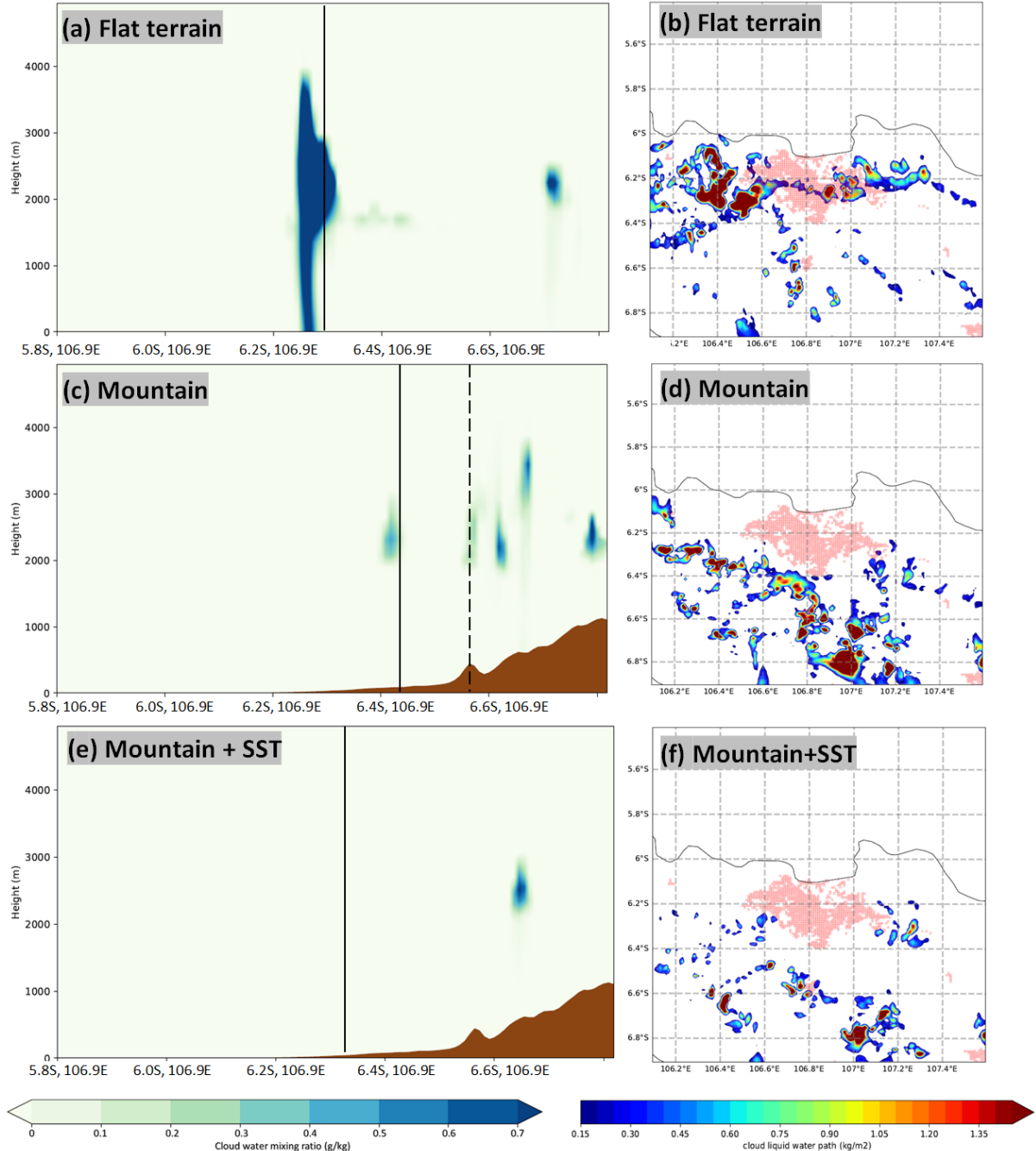


Figure 4.10 Vertical cross-section of cloud water mixing ratio + rainwater mixing ratio (left panel) and horizontal plot of cloud liquid water path (right panel) for the simulations of: (a and b) flat terrain; (c and d) realistic case or with the mountains present; and (e and f) realistic case with increased SST. Maps are shown for the model outputs at 15:00 LT. Vertical black line indicates the SB front location. Vertical black dashed line indicates the location of mountain-induced upward motion. Red shades indicate the grid cells read as urban area.

The presence of mountains results in a slower vertical velocity in the SB front compared to the flat terrain simulation. As the mountain flow accelerates the SB, the SB moves further inland and therefore the SB front is located closer to the countryside (see section 4.2.1). Most of the city area becomes colder as the SB carries colder air from the sea, which in turn leads to a less buoyant boundary layer, although the SB should bring more humidity inducing a more buoyant atmosphere. In the previous hour, the boundary layer is drier when mountains are present compared to the flat terrain (see section

4.4 for further comparisons). Together, these facts result in thinner cloud formation in the vertical plane when mountains are present, compared to flat terrain condition. In this case, another upward motion in the south (around 15 km) of the SB front is present. This motion is the part of mountain waves induced by rising and descending air when the SB encounters mountain obstacles. This mountain-induced upward motion also induces another cloud cell formation, next to the cloud cell induced by the SB front (see figure 4.10.c).

Increasing the SST by 3K in the realistic case simulation results in cloudless conditions over Jakarta. Figure 4.8.f shows that clouds are only visible over the downslope of the mountain. This marks that the clouds are more likely induced by mountain waves. Meanwhile, the model simulation did not capture the cloud formed in the SB front. As discussed earlier, the increase of SST results in higher stability conditions and therefore weaker convection. Thus, it can be concluded that, apart from delaying the SB inland movement, the increase of SST also results in less clouds associated with the SB.

Figure 4.11 shows the cloud parameters resulted from the increase of all urban factors simultaneously and without the increase of building height, which enables us to compare these two factor combinations. The mountain-induced updraft is located closer to the SB front (around 8 km from the SB front) when we increase the urban factors (see figure 4.11.a and c compared to 4.10.c). The extra heat over the city, caused by the increased built-up area and anthropogenic heat, increases surface forcing in the downslope of the mountain. This greater buoyancy could create more turbulent waves that propagate in a greater horizontal distance over the downslope, which in our case takes place in the non-urban area in the south of Jakarta city. Therefore, convection tends to form over that area. The interaction between SB front and mountain waves enhances the convective activity (Joseph et al., 2008). This leads to thicker cloud formation over the non-urban area laying on the downslope of the mountains in the south of Jakarta, with the elevation 100 m to 200 m (figure 4.11.b).

As discussed in section 4.3, when increasing the urban factors without increasing of building height, there is an updraft induced by the UHI in front of the SB front. Meanwhile, the UHI-induced updraft is not present when we increase the building height with the other urban factors. The maximum SB front updraft velocity with the increase of building height is higher, meaning that the primary updraft without the interaction with UHI-induced updraft is higher. Nevertheless, the map of cloud liquid water path does not show thicker clouds formed compared to unchanged building height condition. This is because in the level of 500 m to 1000 m, the boundary layer is slightly drier compared to the unchanged building height, despite a higher updraft velocity in the SB front (see section 4.4). However, the cloud lines are located closer to the south of the city as the SB inland movement is delayed (figure 4.11.d). Moreover, we have less enhanced convective cloud formation over the slope of the mountain compared to the unchanged building height. Since the delayed SB front is still located in the border or urban and non-urban area, therefore the interaction between the SB front and mountain-induced waves is less intense.

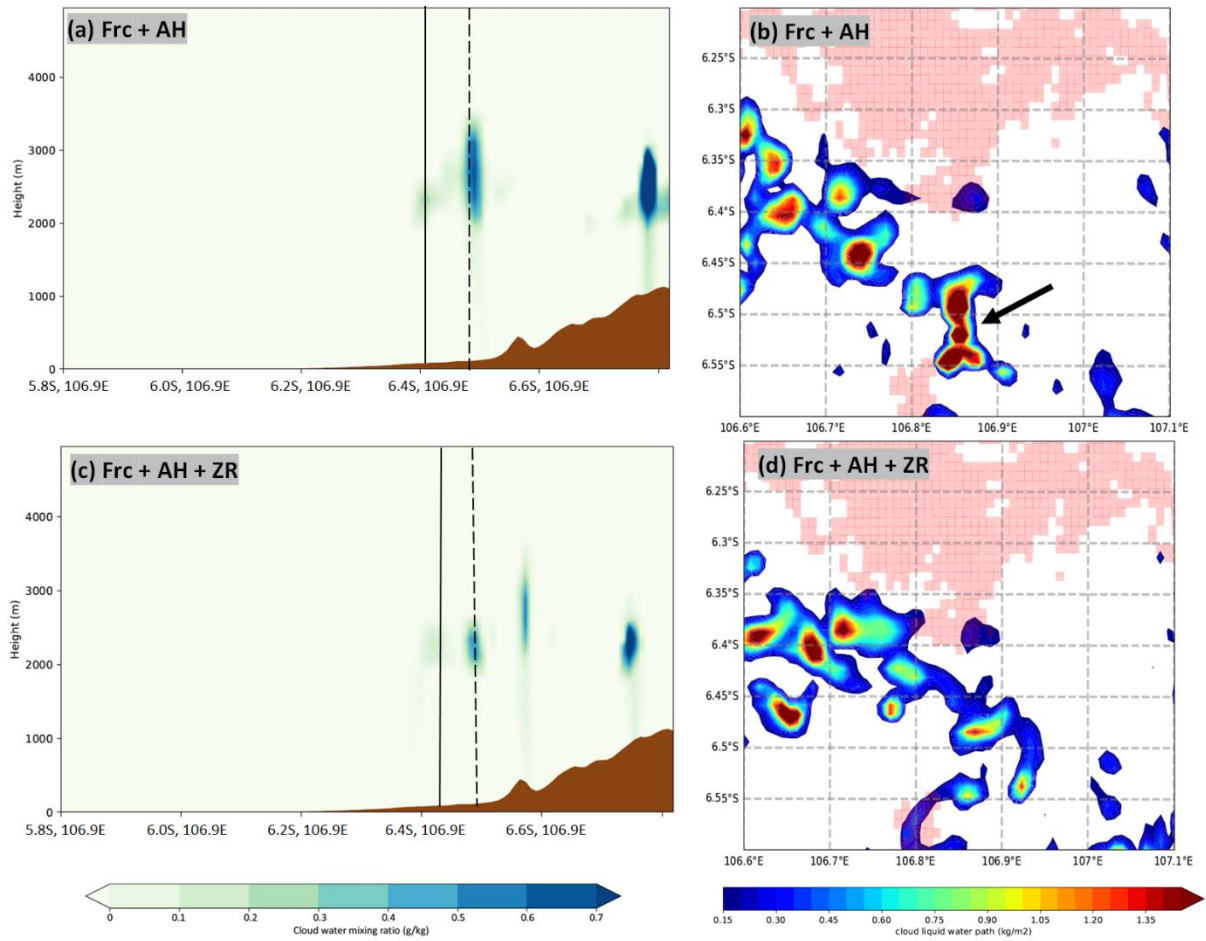


Figure 4.11 Vertical cross-section of modelled cloud water mixing ratio + rainwater mixing ratio (left panel) and horizontal plot of cloud liquid water path (right panel) for the simulations of: (a and b) realistic case with increased built-up fraction and anthropogenic heat in the urban area; and (c and d) realistic case with increased built-up fraction, anthropogenic heat, and building height in the urban area. Maps are shown for the model outputs at 15:00 LT. Vertical black line indicates the SB front location. Vertical black dashed line indicates the location of mountain-induced upward motion. Red shades indicate the grid cells read as urban area. Black arrow indicates the clouds induced by the mountain waves over the non-urban area in the south of Jakarta.

Furthermore, the results presented in this study are only based on one SB day, i.e. the 9th August 2018, occurring during the dry month. The synthesis of effects of mountain flow, urban factors, SST increase and most influential factor combinations on the SB parameters, boundary layer, and cloud formation is presented in table 4.3. In order to obtain more reliable results representing the general influence of urban-related factors, orography, and SST on the SB circulation in Jakarta, more study cases are necessary. These might include the SB events occurring during the rainy seasons (December, January, and February). For urban physics scheme, this study used single-layer urban canopy model with the simplified urban geometry, which is not capable to estimate heat fluxes from building features and ground separately. Meanwhile, the multi-layer scheme, Building Effect Parameterization (BEP, Martilli et al., 2002) can solve the energy budget from different surfaces and calculate the turbulence induced by building features. The next generation of BEP, i.e. Building Energy Model (BEM, Salamanca and Martilli, 2010) even computes the building energy consumption sourced from heating or cooling system, which can accurately represent the heat budget in urban area.

Table 4. 3. Synthesis of the effects of mountain flow, urban factors, SST increase, and most influential factor combinations to SB properties. Up arrows indicate an increase. Down arrows indicate a decrease. Smaller arrows indicate a slight increase/decrease. “NSC” means no significant change.

Factors		Urban air temperature	Urban moisture	SB speed	Sensible heat flux	PBL height	Clouds
Mountain flow	Compared to flat terrain simulation Mountains present (realistic condition)	↓	Drier	↑ (1.8x)	↑	↓	cloudless
Increase of building height (ZR)		↓	NSC	↓ (0.9x)	↓	↓	NSC
Increase of urban built-up fraction (FRC)		↑	Drier	NSC	↓	↑	NSC
Increase of anthropogenic heat emission (AH)		↑	NSC	NSC	↑	↑	NSC
Increase of SST		↑	Drier	↓ (0.6x)	↓	↑	cloudless
FRC + AH		↑	Moister	NSC	↑	↑	enhanced convection and cloud formation in non-urban area (south to Jakarta city)
ZR + FRC + AH		↓	Moister	↓ (0.9x)	↓	↓	clouds closer to the southern part of Jakarta city

5. Conclusion

This study investigated the influences of the interactions between sea breeze (SB), mountain flow, urban-related factors, and the increase of sea surface temperature (SST) on the boundary-layer dynamics and cloud formation in Jakarta. To identify these influences, we simulated the SB by modifying the selected factors and their combinations, using the Weather Research and Forecasting (WRF) model coupled with the single-layer urban canopy model (SLUCM).

The evaluation of parameterization schemes showed that pairing the PBL YSU (non-local) and land surface Noah-MP schemes was found best to reproduce temperature and wind during the SB event, considering the statistical evaluation scores and the wind patterns at the SB passage. However, the MYJ (local) PBL scheme resulted in a lower cold bias of surface air temperature, although YSU better reproduced wind speed and direction. Land surface Noah-MP has a better agreement with observation compared to Noah. Additionally, the model simulations could reproduce two updraft systems in the SB front. The primary one is located adjacent to the SB front due to convergence between land and sea air masses, and the second is an updraft in the cold air behind the SB front formed due to mass conservation.

We calculated the SB strength using a scaling formula to compare the effects of changing certain factors on the SB. Among the selected urban-related variables, only increasing the building height slightly delayed the SB as it caused the lower sensible heat flux over the whole urban area and,

therefore, colder surface temperature. Increasing the urban built-up fraction decreased the temperature only at the area where the SB is active, indicating that it could store more cold air transported by SB than a less built-up urban area. The increase of anthropogenic heat emission resulted in a slight increase of urban sensible heat flux during the daytime, leading to a slight increase in surface air temperature.

The orography was found to have an important role in SB landward propagation. According to the scaling analysis, mountain-induced flow enhanced the SB speed by a factor of two compared to flat terrain simulation. As the accelerated SB rapidly reduced the city air temperature, the surface forcing around the SB front weakened, as well as the convection. This resulted in thinner cloud formation compared to the flat terrain simulation. By increasing the SST, the sea-land thermal contrast became lower, resulting in a slower SB speed. As the SB is delayed, the boundary layer over the city is drier and less well-mixed. This implies that a higher SST resulted in a higher boundary layer stability, weaker convection, and therefore a cloudless condition during the SB event.

Factor separation analysis showed that increasing the urban built-up fraction and anthropogenic heat emission simultaneously resulted in the fastest SB inland movement due to the extra heat over the city. This led to a moister and deeper boundary layer over the urban area. The model captured an urban-induced updraft, leading to an interruption on the updraft velocity in the SB front. As the SB propagated further to the south, it interacted with the mountain-induced waves. It, therefore, created thicker cloud formation over the non-urban area laying above the downslope of the mountain. Increasing the building height simultaneously with the other selected urban factors resulted in higher surface friction which added up thermal instability and strengthened the primary updraft. The cloud lines are located closer to the southern part of Jakarta city as the SB is slightly delayed.

All in all, the increase of urban factors influences the location and enhancement of clouds over Jakarta during a sea breeze event. In contrast, the increase of SST causes a cloudless condition. Since many studies projected the increase of urban factors and SST in the future, these findings might be important to consider. However, our results and conclusions are based on one SB day, which might not be sufficient to represent the general influence of urban surface parameters, mountain flow, and SST on the SB properties in Jakarta. Moreover, this study used a single-layer urban canopy model with simplified urban geometry, which is probably not as good as the other advanced schemes to represent the dynamical processes in the urban canopy. Therefore, for future studies, we would like to suggest including multiple SB days and using the other scheme that can better consider the features in the urban environment, e.g., building energy fluxes.

Acknowledgments

I would first like to thank my supervisor Gert-Jan Steeneveld for his dedicated support and very kind supervision. I would also want to thank Reinder Ronda for his kind help in solving the model technical issues. I want to thank the MAQ thesis ring moderators and my thesis colleagues for insightful feedback and very nice company during thesis work. I want to thank the European Centre for Medium-Range Weather Forecasts (ECMWF) and the Indonesian Agency for Meteorology, Climatology, and Geophysics (BMKG) for providing the data used in this study.

References

- Arellano, J., van Heerwaarden, C., van Stratum, B., & Dries, K. (2015). *Atmospheric boundary layer: Integrating air chemistry and land interactions*.
- Arrillaga, J. A., Yagüe, C., Sastre, M., & Román-Cascón, C. (2016). A characterisation of sea-breeze events in the eastern Cantabrian coast (Spain) from observational data and WRF simulations. *Atmospheric Research*, 181, 265–280.
<https://doi.org/https://doi.org/10.1016/j.atmosres.2016.06.021>
- Bhati, S., & Mohan, M. (2016). WRF model evaluation for the urban heat island assessment under varying land use/land cover and reference site conditions. *Theoretical and Applied Climatology*, 126(1), 385–400. <https://doi.org/10.1007/s00704-015-1589-5>
- Boadh, R., Satyanarayana, A. N. V., Rama Krishna, T. V. B. P. S., & Madala, S. (2016). Sensitivity of PBL schemes of the WRF-ARW model in simulating the boundary layer flow parameters for their application to air pollution dispersion modeling over a tropical station. *Atmósfera*, 29(1), 61–81. <https://doi.org/https://doi.org/10.20937/ATM.2016.29.01.05>
- Borne, K., Chen, D., & Nunez, M. (1998). A method for finding sea breeze days under stable synoptic conditions and its application to the Swedish west coast. *International Journal of Climatology*, 18(8), 901–914. [https://doi.org/https://doi.org/10.1002/\(SICI\)1097-0088\(19980630\)18:8<901::AID-JOC295>3.0.CO;2-F](https://doi.org/https://doi.org/10.1002/(SICI)1097-0088(19980630)18:8<901::AID-JOC295>3.0.CO;2-F)
- Chen, F., Kusaka, H., Bornstein, R., Ching, J., Grimmond, C. S. B., Grossman-Clarke, S., Loridan, T., Manning, K. W., Martilli, A., Miao, S., Sailor, D., Salamanca, F. P., Taha, H., Tewari, M., Wang, X., Wyszogrodzki, A. A., & Zhang, C. (2011). The integrated WRF/urban modelling system: development, evaluation, and applications to urban environmental problems. *International Journal of Climatology*, 31(2). <https://doi.org/10.1002/joc.2158>
- Comin, A. N., & Acevedo, O. C. (2017). Numerical Simulation of Sea Breeze Convergence over Antarctic Peninsula. *Advances in Meteorology*, 2017, 7686540.
<https://doi.org/10.1155/2017/7686540>
- Darmanto, N. S., Varquez, A. C. G., Kawano, N., & Kanda, M. (2019). Future urban climate projection in a tropical megacity based on global climate change and local urbanization scenarios. *Urban Climate*, 29. <https://doi.org/10.1016/j.uclim.2019.100482>
- Ek, M. B., Mitchell, K. E., Lin, Y., Rogers, E., Grunmann, P., Koren, V., Gayno, G., & Tarpley, J. D. (2003). Implementation of Noah land surface model advances in the National Centers for Environmental Prediction operational mesoscale Eta model. *Journal of Geophysical Research: Atmospheres*, 108(D22). <https://doi.org/https://doi.org/10.1029/2002JD003296>
- Ferdiansyah, M. R., Inagaki, A., & Kanda, M. (2020). Detection of sea-breeze inland penetration in the coastal-urban region using geostationary satellite images. *Urban Climate*, 31, 100586.
<https://doi.org/https://doi.org/10.1016/j.uclim.2020.100586>
- Firman, T. (2002). Urban development in Indonesia, 1990–2001: from the boom to the early reform era through the crisis. *Habitat International*, 26(2), 229–249.
[https://doi.org/https://doi.org/10.1016/S0197-3975\(01\)00045-5](https://doi.org/https://doi.org/10.1016/S0197-3975(01)00045-5)
- Freitas, E. D., Rozoff, C. M., Cotton, W. R., & Dias, P. L. S. (2007). Interactions of an urban heat island and sea-breeze circulations during winter over the metropolitan area of São Paulo, Brazil. *Boundary-Layer Meteorology*, 122(1), 43–65. <https://doi.org/10.1007/s10546-006-9091-3>
- Governor of Special Capital Region of Jakarta. (2014). *Peraturan Daerah Provinsi Daerah Khusus Ibukota Jakarta Nomor 1 Tahun 2014 tentang Rencana Detail tata Ruang dan Peraturan Zonasi*.

Retrieved from <https://pelayanan.jakarta.go.id/download/regulasi/peraturan-daerah-nomor-1-tahun-2014-tentang-rencana-detail-tata-ruang-dan-peraturan-zonasi.pdf>

- Hadi, T. W., Horinouchi, T., Tsuda, T., Hashiguchi, H., & Fukao, S. (2002). Sea-Breeze Circulation over Jakarta, Indonesia: A Climatology Based on Boundary Layer Radar Observations. *Monthly Weather Review*, 130(9), 2153–2166. [https://doi.org/10.1175/1520-0493\(2002\)130<2153:SBCOJI>2.0.CO;2](https://doi.org/10.1175/1520-0493(2002)130<2153:SBCOJI>2.0.CO;2)
- Helmis, C. G., Asimakopoulos, D. N., Deligiorgi, D. G., & Lalas, D. P. (1987). Observations of sea-breeze fronts near the shoreline. *Boundary-Layer Meteorology*, 38(4), 395–410. <https://doi.org/10.1007/BF00120854>
- Henkes, A., Fisch, G., Machado, L. A. T., & Chaboureau, J.-P. (2021). Morning boundary layer conditions for shallow to deep convective cloud evolution during the dry season in the central Amazon. *Atmospheric Chemistry and Physics*, 21(17), 13207–13225. <https://doi.org/10.5194/acp-21-13207-2021>
- Hidalgo, J., Masson, V., & Gimeno, L. (2010). Scaling the Daytime Urban Heat Island and Urban-Breeze Circulation. *Journal of Applied Meteorology and Climatology*, 49(5), 889–901. <https://doi.org/10.1175/2009JAMC2195.1>
- Holloway, C. E., & Neelin, J. D. (2009). Moisture Vertical Structure, Column Water Vapor, and Tropical Deep Convection. *Journal of the Atmospheric Sciences*, 66(6), 1665–1683. <https://doi.org/10.1175/2008JAS2806.1>
- Janjic, Z. I. (1994). *The step-mountain Eta coordinate model: Further developments of the convection, viscous layer, and turbulence closure schemes*. (Vol. 122, pp. 927–945).
- Joseph, B., Bhatt, B. C., Koh, T. Y., & Chen, S. (2008). Sea breeze simulation over the Malay Peninsula in an intermonsoon period. *Journal of Geophysical Research*, 113(D20), D20122. <https://doi.org/10.1029/2008JD010319>
- Kato, S., & Yamaguchi, Y. (2005). Analysis of urban heat-island effect using ASTER and ETM+ Data: Separation of anthropogenic heat discharge and natural heat radiation from sensible heat flux. *Remote Sensing of Environment*, 99(1), 44–54. <https://doi.org/https://doi.org/10.1016/j.rse.2005.04.026>
- Kusaka, H., & Kimura, F. (2004). Coupling a single-layer urban canopy model with a simple atmospheric model: Impact on urban heat island simulation for an idealized case. *Journal of the Meteorological Society of Japan*, 82(1), 67–80. <https://doi.org/10.2151/jmsj.82.67>
- Kusaka, H., Kondo, H., Kikegawa, Y., & Kimura, F. (2001). A Simple Single-Layer Urban Canopy Model For Atmospheric Models: Comparison With Multi-Layer And Slab Models. *Boundary-Layer Meteorology*, 101(3), 329–358. <https://doi.org/10.1023/A:1019207923078>
- Liu, J., & Niyogi, D. (2019). Meta-analysis of urbanization impact on rainfall modification. *Scientific Reports*, 9(1). <https://doi.org/10.1038/s41598-019-42494-2>
- Lohmann, U., Lüönd, F., & Mahrt, F. (2016). An introduction to clouds: From the microscale to climate. *An Introduction to Clouds: From the Microscale to Climate*, 1–391. <https://doi.org/10.1017/CBO9781139087513>
- Martilli, A., Clappier, A., & Rotach, M. W. (2002). An Urban Surface Exchange Parameterisation for Mesoscale Models. *Boundary-Layer Meteorology*, 104 (2), 261–304. <https://doi.org/10.1023/A:1016099921195>
- Ministry for National Development Planning of Indonesia. (2010). *Indonesia Climate Change Sectoral Roadmap – ICCSR: Synthesis report*. Retrieved from <https://perpustakaan.bappenas.go.id/e-35>

library/file_upload/koleksi/migrasi-data-publikasi/file/Policy_Paper/synthesis-roadmap_20110217190358_0.pdf

- Miller, S. T. K., Keim, B. D., Talbot, R. W., & Mao, H. (2003). Sea breeze: Structure, forecasting, and impacts. *Reviews of Geophysics*, 41(3). <https://doi.org/10.1029/2003RG000124>
- Niu, G.-Y., Yang, Z.-L., Mitchell, K. E., Chen, F., Ek, M. B., Barlage, M., Kumar, A., Manning, K., Niyogi, D., Rosero, E., Tewari, M., & Xia, Y. (2011). The community Noah land surface model with multiparameterization options (Noah-MP): 1. Model description and evaluation with local-scale measurements. *Journal of Geophysical Research*, 116(D12). <https://doi.org/10.1029/2010JD015139>
- Ogawa, S., Sha, W., Iwasaki, T., & Wang, Z. (2003). A numerical study on the interaction of a sea-breeze front with convective cells in the daytime boundary layer. *Journal of the Meteorological Society of Japan*, 81(4), 635–651. <https://doi.org/10.2151/jmsj.81.635>
- Oke, T. R. (1995). The Heat Island of the Urban Boundary Layer: Characteristics, Causes and Effects. In *Wind Climate in Cities* (pp. 81–107). Springer Netherlands. https://doi.org/10.1007/978-94-017-3686-2_5
- Ookouchi, Y., Uryu, M., & Sawada, R. (1978). A Numerical Study on the Effects of a Mountain on the Land and Sea Breezes. *Journal of the Meteorological Society of Japan. Ser. II*, 56(5), 368–386. https://doi.org/10.2151/jmsj1965.56.5_368
- Powers, J. G., Klemp, J. B., Skamarock, W. C., Davis, C. A., Dudhia, J., Gill, D. O., Coen, J. L., Gochis, D. J., Ahmadov, R., Peckham, S. E., Grell, G. A., Michalakes, J., Trahan, S., Benjamin, S. G., Alexander, C. R., Dimego, G. J., Wang, W., Schwartz, C. S., Romine, G. S., ... Duda, M. G. (2017). The Weather Research and Forecasting Model: Overview, System Efforts, and Future Directions. *Bulletin of the American Meteorological Society*, 98(8), 1717–1737. <https://doi.org/10.1175/BAMS-D-15-00308.1>
- Rafael, S., Rodrigues, V., Fernandes, A. P., Augusto, B., Borrego, C., & Lopes, M. (2019). Evaluation of urban surface parameterizations in WRF model using energy fluxes measurements in Portugal. *Urban Climate*, 28, 100465. <https://doi.org/https://doi.org/10.1016/j.ulclim.2019.100465>
- Rajeswari, J. R., Srinivas, C. V., Rao, T. N., & Venkatraman, B. (2020). Impact of land surface physics on the simulation of boundary layer characteristics at a tropical coastal station. *Atmospheric Research*, 238, 104888. <https://doi.org/https://doi.org/10.1016/j.atmosres.2020.104888>
- Ribeiro, F. N. D., Oliveira, A. P. de, Soares, J., Miranda, R. M. de, Barlage, M., & Chen, F. (2018). Effect of sea breeze propagation on the urban boundary layer of the metropolitan region of São Paulo, Brazil. *Atmospheric Research*, 214, 174–188. <https://doi.org/https://doi.org/10.1016/j.atmosres.2018.07.015>
- Robbany, I. F., Gharghi, A., & Traub, K.-P. (2019). Land Use Change Detection and Urban Sprawl Monitoring in Metropolitan Area of Jakarta (Jabodetabek) from 2001 to 2015. *KnE Engineering*, 4(3). <https://doi.org/10.18502/keg.v4i3.5862>
- Salamanca, F., & Martilli, A. (2009). A new Building Energy Model coupled with an Urban Canopy Parameterization for urban climate simulations—part II. Validation with one dimension off-line simulations. *Theoretical and Applied Climatology*, 99(3), 345. <https://doi.org/10.1007/s00704-009-0143-8>
- Satyanarayana, A. N. V., Lykossov, V. N., Mohanty, U. C., & Machul'skaya, E. E. (2003). Parameterization of Land Surface Processes to Study Boundary Layer Characteristics over a Semi-arid Region in Northwest India. *Journal of Applied Meteorology*, 42(4), 528–540.

[https://doi.org/10.1175/1520-0450\(2003\)042<0528:POLSP>2.0.CO;2](https://doi.org/10.1175/1520-0450(2003)042<0528:POLSP>2.0.CO;2)

- Shen, C., Chen, X., Dai, W., Li, X., Wu, J., Fan, Q., Wang, X., Zhu, L., Chan, P., Hang, J., Fan, S., & Li, W. (2019). Impacts of High-Resolution Urban Canopy Parameters within the WRF Model on Dynamical and Thermal Fields over Guangzhou, China. *Journal of Applied Meteorology and Climatology*, 58(5), 1155–1176. <https://doi.org/10.1175/JAMC-D-18-0114.1>
- Stein, U., & Alpert, P. (1993). Factor separation in numerical simulations. *J. Atmos. Sci.*, 50, 2107–2115. [https://doi.org/10.1175/1520-0469\(1993\)050<2107:FSINS>2.0.CO;2](https://doi.org/10.1175/1520-0469(1993)050<2107:FSINS>2.0.CO;2)
- Stephan, K., Kraus, H., Ewenz, C. M., & Hacker, J. M. (1999). Sea-breeze Front Variations in Space and Time. *Meteorology and Atmospheric Physics*, 70(1–2). <https://doi.org/10.1007/s007030050026>
- Steyn, D. G. (1998). Scaling the Vertical Structure of Sea Breezes. *Boundary-Layer Meteorology*, 86(3), 505–524. <https://doi.org/10.1023/A:1000743222389>
- Stull, R. B. (2012). *An Introduction to Boundary Layer Meteorology*. Springer Netherlands. <https://books.google.nl/books?id=2PjrCAAAQBAJ>
- United Nations. (2019). World Urbanization Prospects: The 2018 Revision. In *World Urbanization Prospects: The 2018 Revision*. <https://doi.org/10.18356/b9e995fe-en>
- Varquez, Alvin Christopher G., Nakayoshi, M., & Kanda, M. (2015). The Effects of Highly Detailed Urban Roughness Parameters on a Sea-Breeze Numerical Simulation. *Boundary-Layer Meteorology*, 154(3). <https://doi.org/10.1007/s10546-014-9985-4>
- Varquez, Alvin Christopher Galang, Kiyomoto, S., Khanh, D. N., & Kanda, M. (2021). Global 1-km present and future hourly anthropogenic heat flux. *Scientific Data*, 8(1), 64. <https://doi.org/10.1038/s41597-021-00850-w>
- Wallace, J.M. and Hobbs, P.V. (2006) Atmospheric Science: An Introductory Survey. 2nd Edition, Elsevier, Amsterdam, 404-408.
- Wichink Kruit, R. J., Holtslag, A. A. M., & Tijm, A. B. C. (2004). Scaling of the Sea-Breeze Strength with Observations in the Netherlands. *Boundary-Layer Meteorology*, 112(2), 369–380. <https://doi.org/10.1023/B:BOUN.0000027904.18874.75>
- Yamanaka, M. D. (2016). Physical climatology of Indonesian maritime continent: An outline to comprehend observational studies. *Atmospheric Research*, 178–179, 231–259. <https://doi.org/https://doi.org/10.1016/j.atmosres.2016.03.017>
- Yang, Z.-L., Niu, G.-Y., Mitchell, K. E., Chen, F., Ek, M. B., Barlage, M., Longuevergne, L., Manning, K., Niyogi, D., Tewari, M., & Xia, Y. (2011). The community Noah land surface model with multiparameterization options (Noah-MP): 2. Evaluation over global river basins. *Journal of Geophysical Research*, 116(D12). <https://doi.org/10.1029/2010JD015140>
- Zhang, Y., Yan, D., Wen, X., Li, D., Zheng, Z., Zhu, X., Wang, B., Wang, C., & Wang, L. (2020). Comparative analysis of the meteorological elements simulated by different land surface process schemes in the WRF model in the Yellow River source region. *Theoretical and Applied Climatology*, 139(1), 145–162. <https://doi.org/10.1007/s00704-019-02955-0>

Appendix

Table A. 1. An overview of the model experiments on urban-related factors using factor separation approach. ‘Default’ refers to the initial values of the UCM variables based on current conditions. ‘Modified’ indicates the projected increased values. For ZR, default is 7.5 m and modified is 20 m. For FRC, default is 51% and modified is 90%. For AH, default is 50 Wm⁻² and modified is 70 Wm⁻². For SST, modified is increased value by 3 K.

Scenario name	Variables changed	Mountain	Building height (ZR) (m)	Urban built-up fraction (FRC) (-)	Anthropogenic heat (AH) (Wm ⁻²)	Sea surface temperature (SST) (K)
f ₀	Control	not	default	default	default	default
f ₁	Mountain	present	default	default	default	default
f ₂	ZR	not	modified	default	default	default
f ₃	FRC	not	default	modified	default	default
f ₄	AH	not	default	default	modified	default
f ₅	SST	not	default	default	default	modified
f ₁₂	Mountain, ZR	present	modified	default	default	default
f ₁₃	Mountain, FRC	present	default	modified	default	default
f ₁₄	Mountain, AH	present	default	default	modified	default
f ₁₅	Mountain, SST	present	default	default	default	modified
f ₂₃	ZR, FRC	not	modified	modified	default	default
f ₂₄	ZR, AH	not	modified	default	modified	default
f ₂₅	ZR, SST	not	modified	default	default	modified
f ₃₄	FRC, AH	not	default	modified	modified	default
f ₃₄	FRC, SST	not	default	modified	default	modified
f ₄₅	AH, SST	not	default	default	modified	modified
f ₁₂₃	Mountain, ZR, FRC	present	modified	modified	default	default
f ₁₂₄	Mountain, ZR, AH	present	modified	default	modified	default
f ₁₂₅	Mountain, ZR, SST	present	modified	default	default	modified
f ₁₃₄	Mountain, FRC, AH	present	default	modified	modified	default
f ₁₃₅	Mountain, FRC, SST	present	default	modified	default	modified
f ₁₄₅	Mountain, AH, SST	present	default	default	modified	modified
f ₂₃₄	ZR, FRC, AH	not	modified	modified	modified	default
f ₂₃₄	ZR, FRC, SST	not	modified	modified	default	modified
f ₂₃₅	ZR, AH, SST	not	modified	default	modified	modified
f ₃₄₅	FRC, AH, SST	not	default	modified	changed	modified
f ₁₂₃₄	Mountain, ZR, FRC, AH	present	modified	modified	modified	default
f ₁₂₃₅	Mountain, ZR, FRC, SST	present	modified	modified	default	modified
f ₁₂₄₅	Mountain, ZR, AH, SST	present	modified	default	modified	modified
f ₁₃₄₅	Mountain, FRC, AH, SST	present	default	modified	changed	modified
f ₂₃₄₅	ZR, FRC, AH, SST	not	modified	modified	changed	modified
f ₁₂₃₄₅	Mountain, ZR, FRC, AH, SST	present	modified	modified	changed	modified

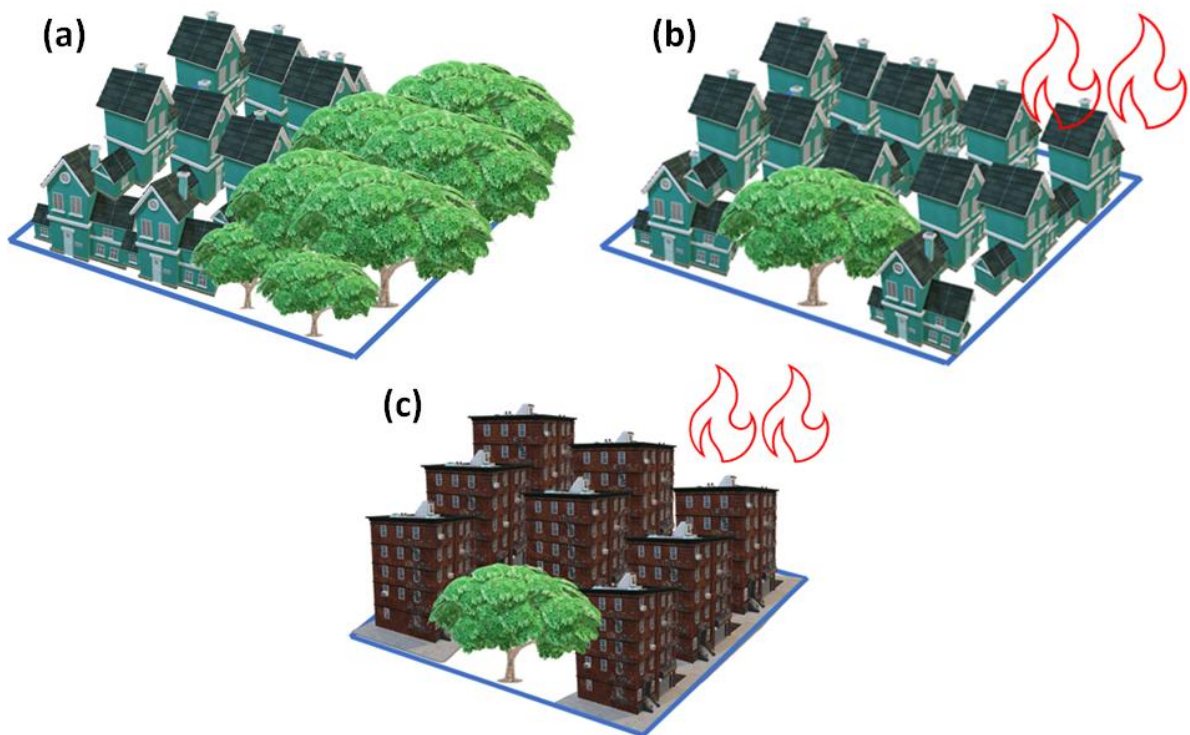


Figure A. 1 Overview of urban characteristics in one model grid cells with: (a) all selected urban factors used in this study are set to their default values; (b) built-up fraction and anthropogenic heat increased; and (c) all urban factors increased

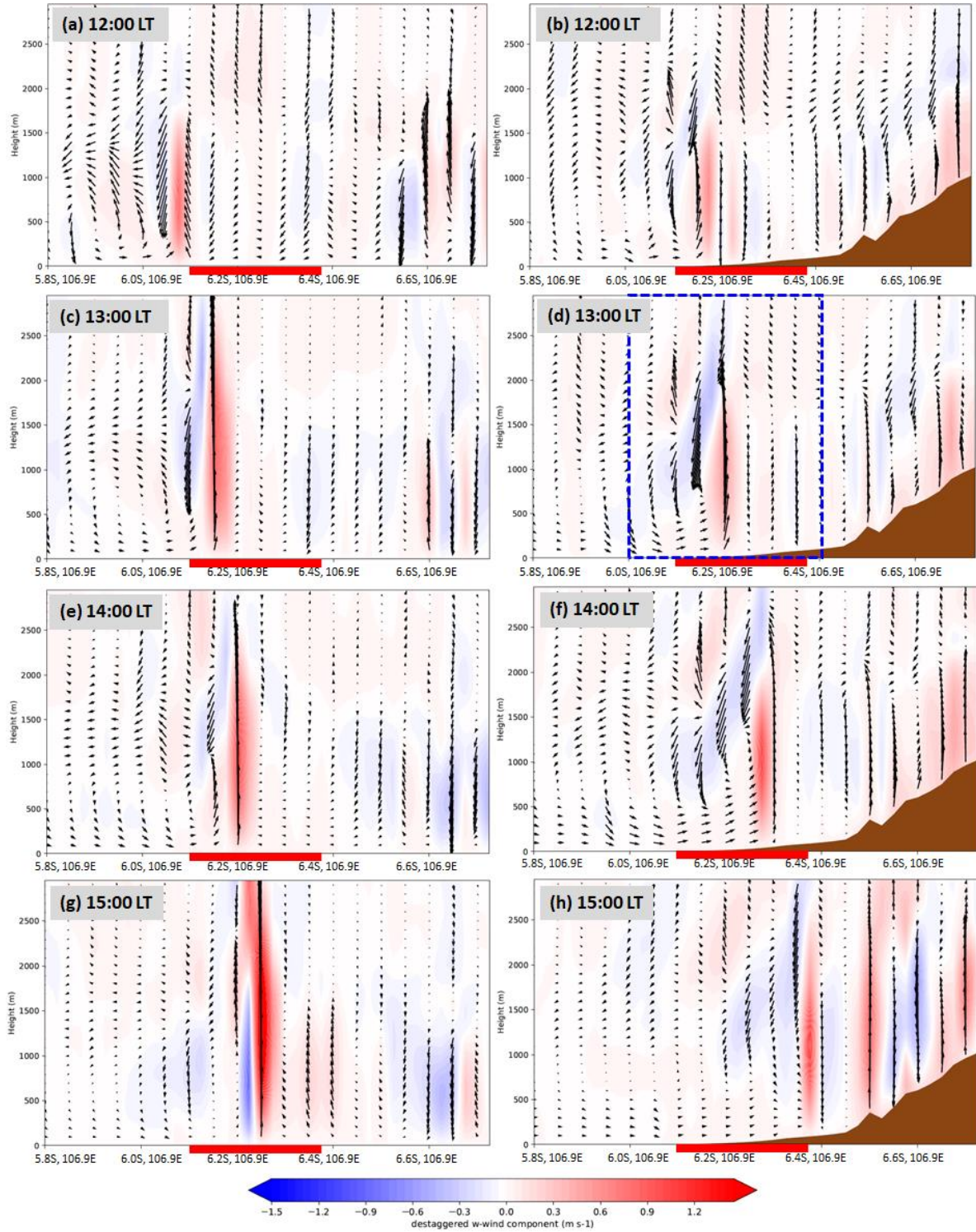


Figure B. 1 Vertical cross-section of vertical velocity (shaded) and vertical winds (arrows) of the model simulations with the flat terrain (left panel) and with mountains (right panel) taken at: (a and b) 12:00 LT, (c and d) 13:00 LT, (e and f) 14:00 LT, and (g and h) 15:00 LT. Red horizontal lines indicate the city area. Blue dashed rectangle indicates the area over which the maximum vertical velocity is calculated.

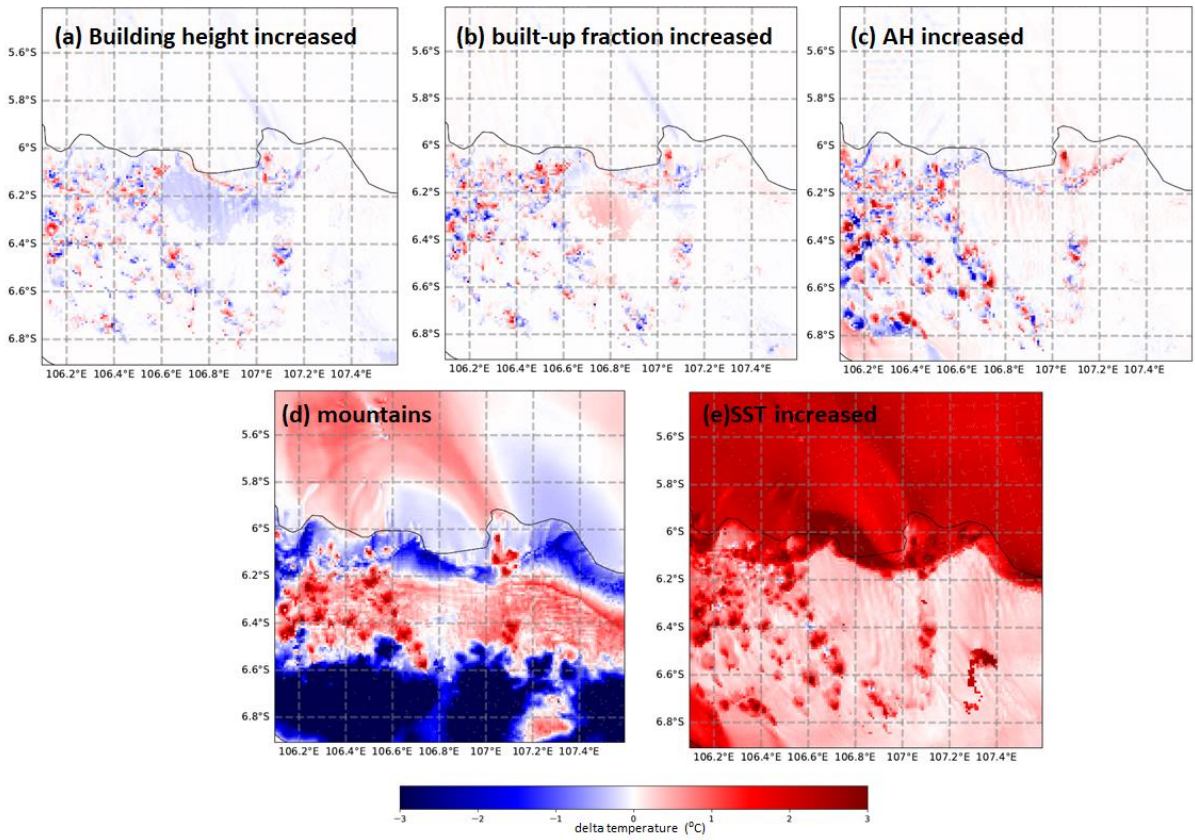


Figure B. 2 The difference of temperature (at 2 m) taken at 13:00 LT between the individual effect of the increase of building height (a), the increase of urban fraction (b), the increase of anthropogenic heat (c), the presence of mountain flow (d), and the increase of sea surface temperature (e), compared to the reference simulation.

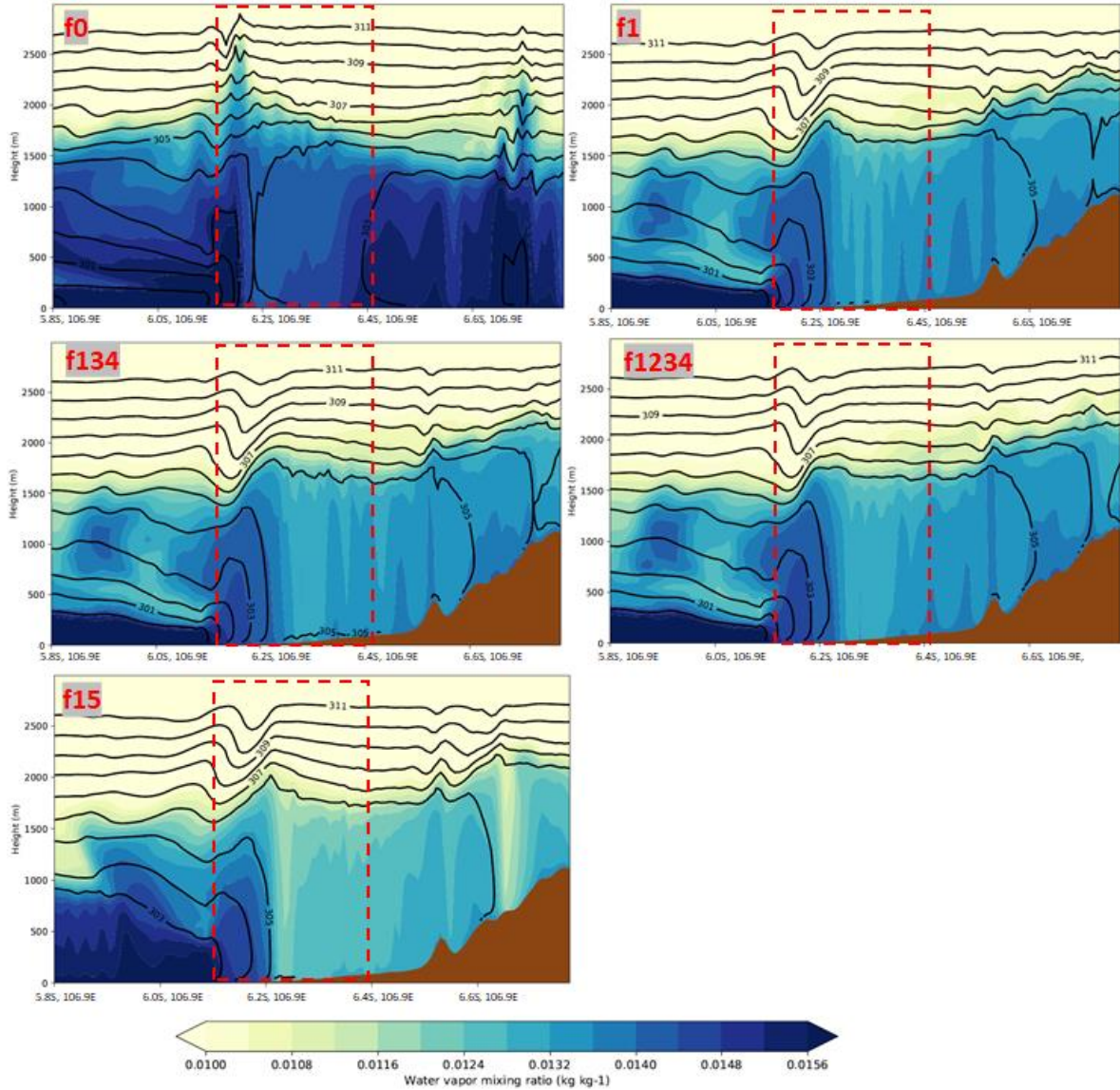


Figure B. 3 Vertical cross-section water vapor mixing ratio (shades) and potential temperature (contours) at 13:00 LT (06:00 UTC) for the model simulations of: flat-terrain, urban factors and SST are set default (f0); a realistic case with mountains presence, urban factors and SST are set default (f1); mountains presence, with urban fraction and anthropogenic heat increased (f134); mountains presence, with building height, urban fraction and anthropogenic heat increased (f1234); and mountains present, with urban factors default, and SST increased (f15). The red rectangle indicates the urban area.

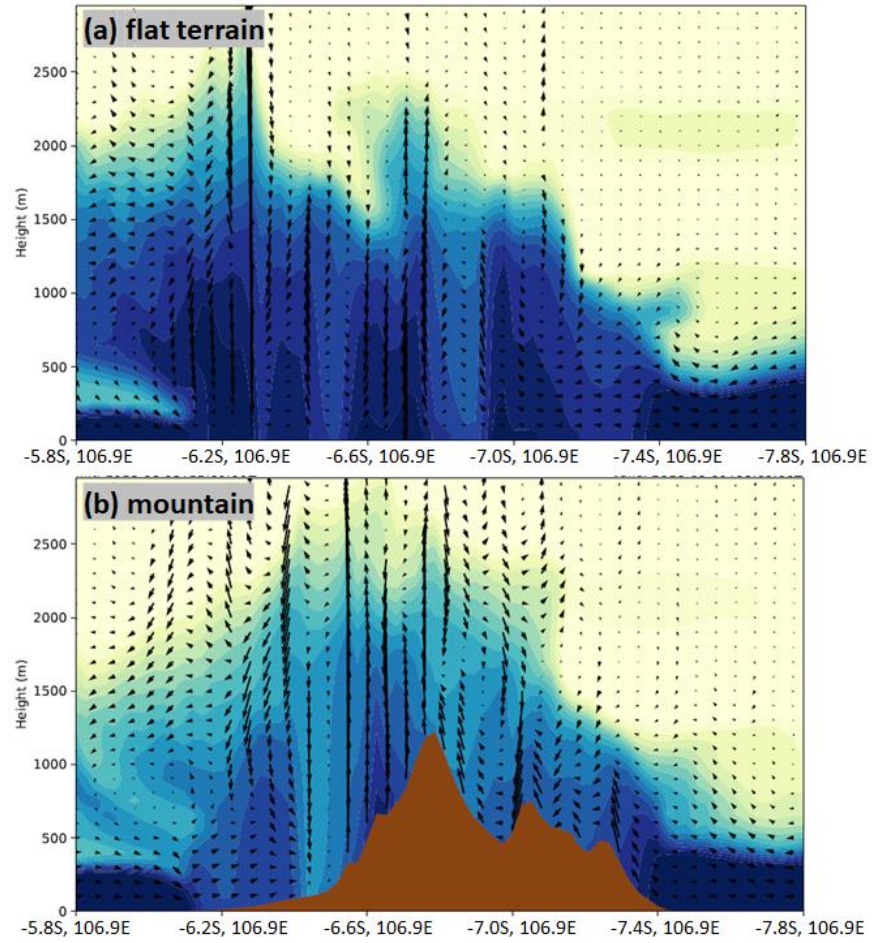


Figure B. 4 Vertical cross-section of water vapor mixing ratio (shades) and vertical winds (arrows) at 13:00 LT for a longer transect of Jakarta, covering the northern sea of Jakarta and the southern sea of West Java Province, taken from simulations with: (a) flat terrain and (b) mountains present.